**SANDIA REPORT**

SAND2018-10820
Unlimited Release
Printed September 2018

# Solid Mechanics Code Verification: Contrasting Classical and Manufactured Reference Solutions

James V. Cox

Prepared by
Sandia National Laboratories
Albuquerque, New Mexico 87185 and Livermore, California 94550

Sandia National Laboratories is a multimission laboratory managed and operated by National Technology and Engineering Solutions of Sandia, LLC, a wholly owned subsidiary of Honeywell International, Inc., for the U.S. Department of Energy's National Nuclear Security Administration under contract DE-NA0003525.

Sandia National Laboratories

Issued by Sandia National Laboratories, operated for the United States Department of Energy by National Technology and Engineering Solutions of Sandia, LLC.

Available to DOE and DOE contractors from
U.S. Department of Energy
Office of Scientific and Technical Information
P.O. Box 62
Oak Ridge, TN 37831

Telephone: (865) 576-8401
Facsimile: (865) 576-5728
E-Mail: reports@osti.gov
Online ordering: http://www.osti.gov/scitech

Available to the public from
U.S. Department of Commerce
National Technical Information Service
5301 Shawnee Rd
Alexandria, VA 22312

Telephone: (800) 553-6847
Facsimile: (703) 605-6900
E-Mail: orders@ntis.gov
Online order: https://classic.ntis.gov/help/order-methods/

SAND2018-10820
September 2018
Unlimited Release

# Solid Mechanics Code Verification: Contrasting Classical and Manufactured Reference Solutions

James V. Cox
Computational Shock Physics
Sandia National Laboratories
P. O. Box 5800
Albuquerque, New Mexico 87185-MS0840

## Abstract

Verification results for Sierra/SM using inexact reference solutions have often exhibited unsatisfactory convergence behavior. With an understanding of the convergence behavior for these types of tests, one can avoid falsely attributing pathologies of the test with incorrectness of the code. Simple theoretical results highlight that for an inexact reference solution two conditions must be met to observe asymptotic convergence. These conditions, and the resulting types of convergence behaviors, are further illustrated with graphical examples depicting the exact, inexact reference, and sequence of numerical solutions as vectors (in a function space). A stress concentration problem is adopted to contrast convergence behaviors when using inexact (classical linear elastic) and exact (manufactured) reference solutions. Convergence is not initially attained with the classical solution. Convergence with the manufactured solution indicates the convergence failure with the classical reference did not result from code error and provides insight on how for this problem asymptotic convergence could be attained with the classical reference solution by modifying the computational models.

# ACKNOWLEDGMENTS

I thank David Lo, Brian Carnes, and George Orient for helpful discussions and encouraging a study on the topic of inexact reference solutions to support Sierra/SM verification. The model problem adapted in this study was initially examined by George Orient and a summer intern, Tyler Alvis and reported in a technical presentation [Orient and Alvis 2017]. I thank George for posing the question of how we could improve on the initial results, which led to the comparison of the results using manufactured and classical solutions presented in this report. I also thank Brian Carnes, Kevin Dowding, and John Red-Horse for reviewing all (or sections) of the document, and Angel Urbina, Walter Witkowski, and Kim Mish for supporting this work.

# TABLE OF CONTENTS

# 1. INTRODUCTION

This report presents a study on the apparent convergence issues that can result when using an inexact reference solution, like a classical linear elasticity solution*. The study was partially motivated by results that have been obtained in developing convergence tests for Sierra/SM but provides supplemental material not contained in the Sierra/SM Code Verification Manual [Sierra/SM Team 2018]. The report provides some analytical relationships and corresponding graphical idealizations to explain the convergence responses that can be observed when using either an exact or inexact reference solution. Then a stress concentration problem is used to compare convergence responses based upon both manufactured (exact) and classical linear elastic (inexact) reference solutions, demonstrating convergence pathologies that can follow from the choice of an inexact reference solution – not a code error.

## 1.1. Background on Sierra/SM Convergence Testing

In 2013 a collaborative effort between the Sierra/SM code team (1542), "V&V department" (1544), and solid mechanics analysts (1550) was initiated to assess and advance the Sierra/SM verification test suite (VERTS). The first study sought to assess the potential of using verification tools developed in 1544 for Sierra/SM code verification, with an emphasis on evaluating the potential use of Encore [Copps and Carnes 2014] to integrate norms of errors in displacement and stress fields. The initial work, presented in a report by Cox and Mish [2013], examined the convergence behavior of Sierra/SM for two classical mechanics problems. The study demonstrated the potential to use Encore for post-processing results for convergence testing but also demonstrated issues that occur when using a classical reference solution that is based upon governing equations which differ from those the finite element code approximates (*i.e.*, the strong form of the equations being approximated). Motivated to provide stronger convergence results, a Mathematica program was developed to manufacture exact solutions to a subset of the nonlinear equations that Sierra/SM approximates [Cox 2013, 2016]. A simple problem with a quadratically varying displacement field was initially used to demonstrate the approach. While Sierra/SM had numerous verification tests in its VERTS, it lacked convergence testing for order of accuracy even with classical solutions. Testing scripts (Python and Bash) and the Mathematica program were further developed to facilitate convergence testing using both classical and manufactured reference solutions.

In Solid Mechanics, the initial input for a manufactured solution consists of a displacement or motion/configuration mapping function. Among the sources of this input [Cox 2013] for a nonlinear solid mechanics code is a displacement field derived from a simpler theory like linear elasticity. Additional approximations may be included either in the theory (*e.g.*, the kinematic approximations of Euler-Bernoulli beam theory), in the solution approach (*e.g.*, Hertzian contact assumptions), or in the numerical evaluation of the solution (*e.g.*, retaining a finite number of terms

---

* An *inexact reference solution* is simply a solution that does not exactly solve the governing equations that the code approximates. In our verification work these have usually been classical solutions of linear elasticity problems, and the Sierra Solid Mechanics (SM) code always solves the fully nonlinear equations of solid mechanics; thus the terms *classical reference solutions* and *inexact reference solutions* are used interchangeably in this report. In a similar manner, for brevity, the terms *manufactured solutions* and *exact solutions* are used interchangeably. Admittedly these simplifying equivalences gloss over the facts that there are some exact solutions to the nonlinear equations of solid mechanics that might be referred to as classical solutions, and one can manufacture a solution for linear elasticity that is an inexact reference for Sierra/SM.

from an infinite series solution) to facilitate using a classical solution as a reference solution, but some can make a manufactured solution more difficult to interpret. For example, manufacturing a solution for Euler-Bernoulli beam theory [Cox 2013, 2016] of a cantilevered beam with an end load leads to a "manufactured problem" without an end shear on the beam. So even when the load is small, the problem does not reduce to the original, familiar beam problem. For a problem manufactured with a linear elastic solution (and having no further approximations to obtain the solution), the problem should reduce to the original linear elastic problem as the load level is reduced. This is fairly straightforward since the nonlinearities that make the exact solution differ from the classical solution disappear as the loading approaches zero [Cox 2013]. This behavior is demonstrated in this report.

## 1.2. Idealized Convergence Plots using Exact and Inexact Reference Solutions

The use of reference solutions from linear elasticity is a natural first step in code verification, but it has some limitations in convergence studies of a nonlinear code. Those limitations are what motivated an examination of the problem presented in this report. Ideally the error in the approximation will satisfy a theoretically derived relationship of the form

$$\|e_h\| = \|u_h - u_{exact}\| = ch^p + O(h^{p+1}) \tag{1}$$

for some constant $c$, where $p$ denotes the theoretical rate of convergence, $h$ is a measure of the element size[*], $u_h$ denotes the approximate solution for element size $h$, $e_h$ denotes the error function associated with the element size $h$, and $||.||$ is a norm (a measure of length or size).

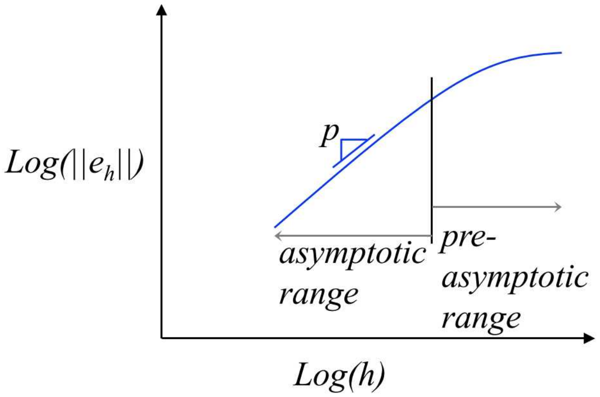

*Figure 1. Convergence with an exact reference solution.*

Figure 1 depicts a hypothetical convergence plot. Note that the response can be divided into two ranges of response, the *pre-asymptotic* and *asymptotic* ranges. As $h$ decreases, the right hand side of Equation (1) asymptotically approaches the first term, $ch^p$. When $h$ is sufficiently small for this first term to "dominate," the approximate solutions are described as being in the *asymptotic range,* and we can express this in the approximation

---

[*] This can be generalized to include time discretization too, but in this study we only consider a spatial discretization.

$$\|e_h\| \approx ch^p \tag{2}$$

Thus the theoretical rate of convergence ($p$) is often referred to as the *asymptotic rate of convergence,* and the observed value can be estimated from the slope on a log-log plot of the convergence data ($\|e_h\|$ *vs.* $h$). Prior to $h$ being small enough to make this approximation, the higher order terms on the right hand side of Equation (1) can affect the observed rate of convergence (*e.g.*, slope of the secant between successive approximations), as depicted in the pre-asymptotic range. The delineation between the two regions is subjective, depending upon what level of accuracy in the observed convergence rate is considered sufficient. In some cases, even the coarsest mesh results examined might be considered to be within the asymptotic range.

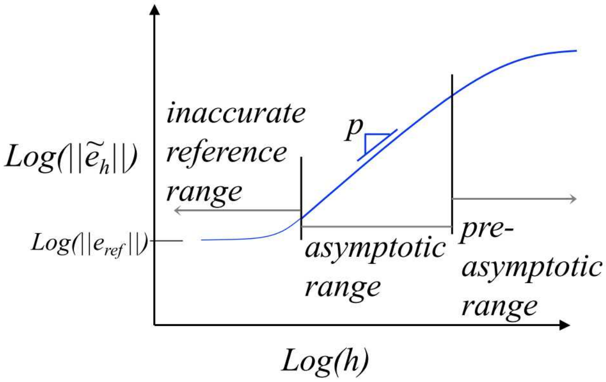

*Figure 2. Convergence with an inexact reference solution.*

Now consider the case where our reference solution is not exact. Figure 2 depicts a hypothetical convergence plot for this case. Assume the code being verified is correct (*i.e.*, is convergent to the exact solution) and that a sequence of results for mesh refinements are examined. Note that there are three characteristic response ranges depicted in this plot. The first two ranges are consistent with those observed with an exact reference solution, though for some cases one or the other may not be apparent in the observed response. The third range, the *inaccurate reference range*, as named is the range over which the inexact reference solution is too inaccurate to yield an accurate estimate of the error or a representative rate of convergence. In the limit, the numerical solution converges to the exact solution, not the inexact reference solution, so the curve approaches a constant value equal to the error in the reference solution. The sketch depicts the error monotonically approaching a constant value; as explained in the next section monotonic convergence to this value is not always the case. Of course these statements are correct only if the code does not have an error that affects the convergence. For results that have this last range of response and for which one does not know the exact solution, it is not clear from a typical test if the apparent lack of convergence for the finest meshes is simply a pathology of using an inaccurate reference solution or if it is indicative of a coding error. This uncertainty, combined with the test only addressing the linear elastic response (in this case), are why tests with an inexact reference solution are generally considered to be less rigorous, though not without value. Note that in some cases with an inexact reference solution, it is difficult to obtain numerical results in which an apparent asymptotic range exists (*i.e.*, the inaccurate reference region can even over-lap the pre-asymptotic range).

The next section of this report examines the convergence with an inexact reference solution in more detail. For the reader who found the above two figures to present common knowledge or who is willing to accept them without further explanation, Section 2 can be skipped; it presents both simple analytical and graphical explanations of the trends in Figure 2. Section 3 presents a stress concentration problem, both its classical and manufactured reference solutions, and numerical models used in the verification testing. The problem is a classic stress concentration problem of a circular hole in an infinite plate. Since Sierra/SM is purely a three-dimensional code, we solve the plane strain version of the problem with one element through the thickness. Section 4 presents results for verification tests using both reference solutions. Lastly, Section 5 presents a closing summary.

# 2. APPARENT CONVERGENCE BEHAVIORS WITH AN INEXACT REFERENCE SOLUTION

The first subsection of this section presents a relatively simple theoretical explanation of the convergence behaviors depicted Figure 2. The next subsection seeks to explain the same behaviors graphically, representing the exact solution, reference solution, and sequence of numerical solutions as vectors in a space.

## 2.1. Simple Theoretical Explanation of Apparent Convergence Behaviors

Equation (1) gave the theoretically derived expression (ideally) of the solution error as a function of the discretization size ($h$). While this expression is consist with Figure 1, it does not provide direct insight to the illustrated response with an inexact reference solution (depicted in Figure 2), or variations there of that might exhibit non-monotonic convergence to a fixed error. This section provides simple analytical explanations of the three response regions for that general case.

Let $u_{ref}$ denote the reference solution and $e_{ref}$ denote the error in this solution[*], as given by

$$e_{ref} = u_{exact} - u_{ref} \tag{3}$$

Now we can rewrite Equation (1) as

$$\|e_h\| = \|u_h - e_{ref} - u_{ref}\| \tag{4}$$

Let $\tilde{e}_h$ denote the *apparent error*, *i.e.*, relative to our inexact reference solution, given by

$$\tilde{e}_h = u_h - u_{ref} \tag{5}$$

Note that this is not the *true error*, but it is an apparent error measured relative to an approximate analytical reference solution. The approximate reference solution is essentially a simpler, attainable solution to a *surrogate mathematical model* that we hope is sufficiently close to the actual mathematical model (*i.e.*, governing equations) for the solution to serve as a useful reference for error measurements. The most common case for this surrogate mathematical model are the equations of linear elasticity, possibly with further simplifying assumptions (*e.g.*, in the Hertzian approach to contact or kinematic assumptions in structural theories like Euler-Bernoulli beam theory).

Equation (4) can now be written as

$$\|e_h\| = \|\tilde{e}_h - e_{ref}\| \tag{6}$$

Assuming that the numerical solutions are converging[†] to the exact solution (*i.e.*, $\|e_h\| \to 0$), as Equation (1) implies, then

---

[*] The sign convention used here is defined to be consistent with the apparent error but does not affect the final results.

[†] Note that the term *convergence* is used to refer to multiple quantities in this document. The primary usage is to describe the *convergence* of a sequence of numerical solutions to an exact solution. We also refer to the *apparent convergence* to a reference solution, though sometimes the modifier "apparent" is omitted for brevity. Finally, we also refer to the *convergence* of the apparent error as given in Equation (7). The combination of the three is a key theme to

$$\lim_{h \to 0} \tilde{e}_h = e_{ref} \tag{7}$$

This is consistent with the *inexact reference range* depicted in Figure 2.

To consider the conditions for which one might observe asymptotic convergence with an inexact reference solution, let's examine how the norm of the apparent error can be expressed in terms of the norm of the actual error. Starting from Equation (5) we can take the norm of both sides as

$$\|\tilde{e}_h\| = \|u_h - u_{ref}\| \tag{8}$$

If we subtract and add the exact solution, $u_{exact}$, from the two terms on the right hand side, respectively we can write

$$\|\tilde{e}_h\| = \|e_h + e_{ref}\| \tag{9}$$

By the triangle inequality this can be written as

$$\|\tilde{e}_h\| \leq \|e_h\| + \|e_{ref}\| \tag{10}$$

in which equality only occurs if $e_h$ and $e_{ref}$ are in the "same direction." Now if we express the norm of the true error using Equation (1) we can write

$$\|\tilde{e}_h\| \leq ch^p + O(h^{p+1}) + \|e_{ref}\| \tag{11}$$

This relationship shares the non-asymptotic term taken from Equation (1) but has a second term, the size of the error in the reference solution. As such there are two constraints on obtaining an apparent asymptotic response. If we assume we are in the asymptotic range, we can neglect the highest order term. We have the approximate inequality given by

$$\|\tilde{e}_h\| \lesssim ch^p + \|e_{ref}\| \tag{12}$$

We already have established the asymptotic result that as $h \to 0$ the apparent error approaches the error in the reference solution, and thus the norms would be equal in the limit. The more interesting aspect of the above approximation is that if $\|e_{ref}\| \ll ch^p$ , *i.e.*, the error in the reference solution is negligible compared to the asymptotic error relative to the exact reference solution, we have an approximation, similar to Equation (1); the caveat here is that we have an approximate inequality, *i.e.*, an approximate bound. However the inequality was simply a result of the order in which we introduced the two simplifying approximations. Note that for the case when the error in the reference solution is relatively small, Equation (9) could have been approximately expressed as

$$\|\tilde{e}_h\| \approx \|e_h\| \tag{13}$$

---

this section: a numerical solution can initially exhibit *apparent convergence* (sometimes even asymptotic convergence) to an inexact reference solution, but eventually it will di*verge* to a fixed error – the error in the reference solution. When the later occurs, the numerical solution appears to be *divergent*, even when it is *convergent* to the exact solution.

and then when in the asymptotic range our apparent error would appear to exhibit asymptotic behavior. Inequality (11) however simultaneously shows both issues that must be met to observe asymptotic convergence when using an inexact reference solution: (1) the solution must be in the asymptotic range (as measured by the exact solution), and (2) the error in the reference solution must be so small that the size of apparent error vector is almost identical to the size of the actual error vector. Note that the higher order terms by definition diminish with mesh refinement, however the effect of the error in the reference solution increases with mesh refinement. These two constraints on observing the asymptotic response are apparent in Figure 2. The *pre-asymptotic range* corresponds to when the $O(h^{p+1})$ term is too large relative to $ch^p$, and the *inaccurate reference range* corresponds to when the $||e_{ref}||$ is too large relative to $ch^p$. As such, the intent in a test with an inexact reference solution is to have some responses in this "sweet spot" where the asymptotic convergence can be observed (*albeit* generally not as precisely as with an exact reference solution). We have observed cases with inexact reference solutions in which the asymptotic behavior could and could not be measured (at least with the meshes examined). Among the cases where the asymptotic behavior could not be measured were several contact verification tests based upon the solution approach of Hertz [Sierra/SM team 2018].

## 2.2. Graphical Explanation of Apparent Convergence Behaviors

Now let's consider a graphical representation of these convergence statements, where we represent numerical and reference solutions as vectors in a function space.* Assume a sequence of mesh refinements for which $h_{i+1}=h_i/2$. We concisely denote the $i^{th}$ numerical solution as

$$u_i = u_h(h_i) \tag{14}$$

and let the corresponding apparent and true error vectors be denoted as

$$\tilde{e}_i = \tilde{e}_h(h_i) \quad and \quad e_i = e_h(h_i) \tag{15}$$

The function space that our solution lives in is inherently infinite dimensional†, but for illustrative purposes the following figures depict the exact solution, reference solution, and sequence of numerical solutions as being vectors in a two-dimensional space (or three-dimensional if the reader prefers that interpretation). The key observations can be illustrated with this level of simplification, because they simply reduce down to geometry. It is the relative orientations of the exact solution, reference solution, and sequence of numerical solution vectors that determine the apparent convergence behavior (and lack thereof) when an inexact reference solution is adopted.

---

[*] In general, the solution to the weak form of the governing equations is assumed to be in a Sobolev space for which a given order of derivative is square integrable over the domain (first order for the solid mechanics problems considered here). In previous Sierra/SM verification work, brief descriptions of these well-known function spaces were given in Cox and Mish [2013] and Sierra/SM team [2018]. For more complete explanations reference the texts of Oden [1979] and Stakgold [1979].

[†] For those less familiar with function spaces, think for example of each basis vector as being a trigonometric function in the Fourier expansion of a particular function, with the coefficient of each trigonometric function representing the coordinate associated with the basis vector. For simplicity, if the trigonometric functions are normalized we have an *orthonormal basis*. As such, each solution vector (a function) can be represented as a unique linear combination of basis vectors (each of which are also functions). The plots can then simply be thought of as schematically depicting the solution vector in terms of its coordinates, though the vector could be represented by other bases.

First consider the simple case of an exact reference solution. Equation (1) would give a convergence in the function space of the solution as depicted by Figure 3. In this depiction the convergence is approximately linear for the finer meshes using a 2-norm, $||.||_2$ (*i.e.*, the size of the error vector reduces by a factor of one half for each mesh refinement from mesh 2 onward[*]). Mesh 1 is outside of the asymptotic range as depicted by $||e_2||_2$ being greater than one half of $||e_1||_2$. (Note that we depict linear convergence simply to be able to show several vectors for the numerical solution; higher order convergence yields extremely small error vectors with fewer mesh refinements).

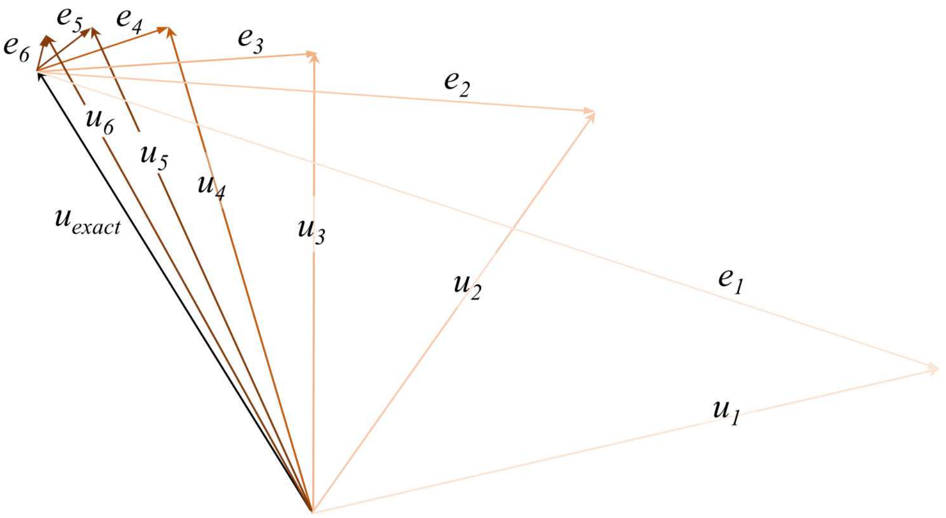

*Figure 3. Convergence to an exact reference solution.*

Now let's consider cases with an inexact reference solution. In the figures that depict these cases, we assume that the numerical solution is converging to the exact solution. As such, the apparent lack of convergence is always due to in an inaccurate reference solution.[†]

---

[*] While these figures are intended to be a schematic representation, if we assume the solutions live in a finite dimensional subspace with an orthonormal basis, it is easy to show that the 2-norms of the coordinates of the vectors are equal to the $L_2$-norms of the functions, thus providing a more tangible connection between the spaces of interest (function spaces) and the two-dimensional schematics. The $L_2$-norm on a domain $\Omega$ is defined as:

$$\|u\|_2 = \sqrt{\int_\Omega u^2 d\Omega}.$$

[†] As previously noted in a real test problem where one does not know the exact solution the lack of convergence could be due to a code error or the use of an inexact reference solution. This uncertainty in that context is what makes a convergence test with an inexact reference, especially if an asymptotic range does not appear to exist, a weaker verification test.

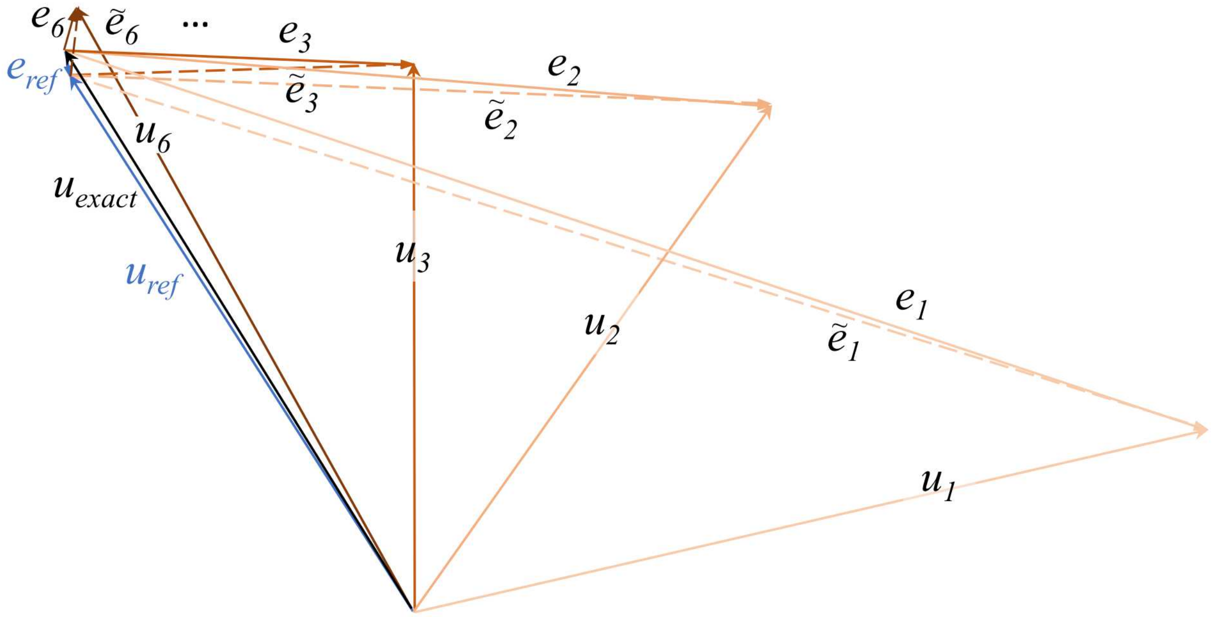

*Figure 4. Convergence showing error and apparent error vectors.*

Figure 4 shows a partial sequence of mesh refinements for a case where the inexact reference solution is relatively close to the exact solution when considering the results and corresponding errors for the coarser meshes (1 through 3). For these three meshes Equation (13) is satisfied, and thus the inexact reference solution is sufficient to reveal asymptotic convergence, however the higher order error terms must be sufficiently small too. Based upon the true error vector sizes, $e_2$ is considerably more than half the size of $e_1$ and thus linear convergence is not yet apparent (*i.e.*, the higher order terms are significant for $e_1$). Error $e_1$ would appear to be in the pre-asymptotic range on a convergence plot. Errors $e_2$ and $e_3$ appear to be in the asymptotic range, the size of $e_3$ halving with mesh refinement. Certainly by mesh 6 the difference between the inexact reference solution and the exact solution would result in the error and apparent error being quite different, thus it would be in the *inexact reference range* of a convergence plot, where the error converges to a fixed value, $||e_{ref}||$.

*Aside:* Note that when we apply the triangle inequality to obtain Inequality (10), we gain a relationship that allows us to express the error in the exact solution in terms of *h*, but we lose the fact that the orientation of the sides of the triangle matter. Specifically while, having $||e_{ref}||$ small is one of two sufficient conditions to attaining an asymptotic range, it is not necessary for all meshes in the sequence. That is it does not have to be as small if the orientation of $e_{ref}$ is as depicted for mesh 3; eventually of course, its size matters since the limit of Equation (7) will hold true, but orientation can cause the effect to occur later with respect to mesh refinement.

The case presented in Figure 4 would have a convergence plot as depicted in Figure 2 , that is with all three response regions and monotonic convergence to a fixed error. Now let’s consider cases that differ from that idealized convergence plot response.

In Figure 5 we consider a case where the apparent error appears to be monotonically converging to the reference solution initially, but from mesh 5 or 6 onward the norm of the apparent error vector would be seen as approaching that of $e_{ref}$, a fixed error value. As such, the numerical solution would be perceived as not converging. The true errors are not depicted in this figure, but their sizes reflect linear convergence from meshes 3 or 4 onward. So while the higher order terms might be small enough to give an asymptotic range for the exact solution, the error in the inexact reference solution would mask the asymptotic behavior. As noted with Inequality (11), both contributions on the right-hand-side (other than $ch^p$) must be relatively small to obtain an *apparent asymptotic range*; in this case only the *pre-asymptotic* and *inaccurate reference* ranges of Figure 2 would be apparent in a convergence plot.

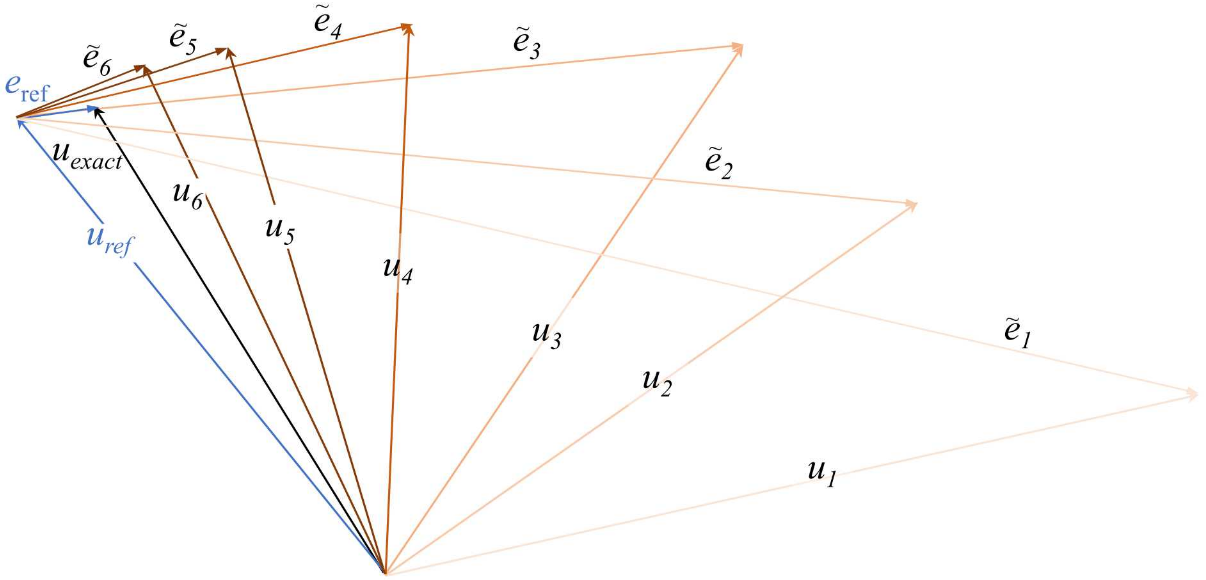

*Figure 5. Initial apparent convergence to an inexact reference solution followed by monotonic convergence to a fixed apparent error.*

Figure 6 presents another case that is similar to the last one except the convergence to the constant error value does not appear to be monotonic, that is initially the numerical solution appears to be converging to the reference solution and then later the apparent error increases. As with the previous case, the numerical solution appears to not converge but approaches a fixed value in a non-monotonic manner. Also like the previous case, while there are coarser mesh results that appear to be converging to the reference solution, the size of the error in the reference solution prevents the observation of an asymptotic response. This is not to say there is not an asymptotic response (as there is to the exact solution); it is just that it can not be observed with an error measurement relative to the inexact reference solution. As we will observe in the results presented in Section 4, in some instances one can reduce the error in the reference solution (*e.g.*, by changing to a more accurate set of boundary conditions or decreasing the level of loading), so that the reference problem is a better surrogate problem to the exact one. This yields a more accurate reference solution, and then the asymptotic convergence can be observed.

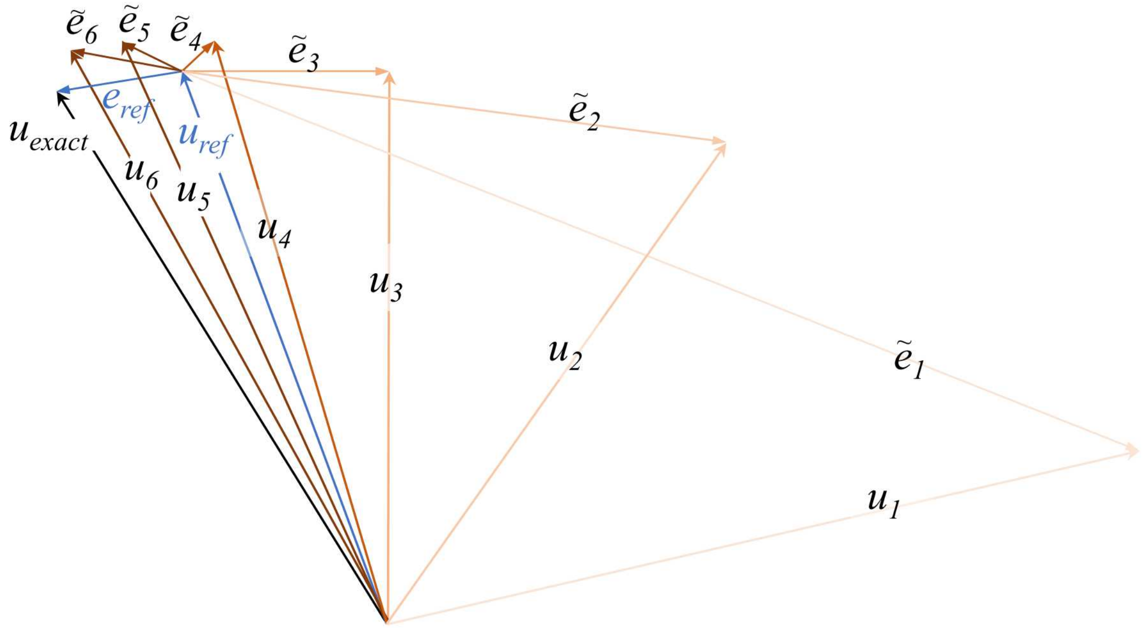

*Figure 6. Initial apparent convergence to an inexact reference solution followed by non-monotonic convergence to a fixed apparent error.*

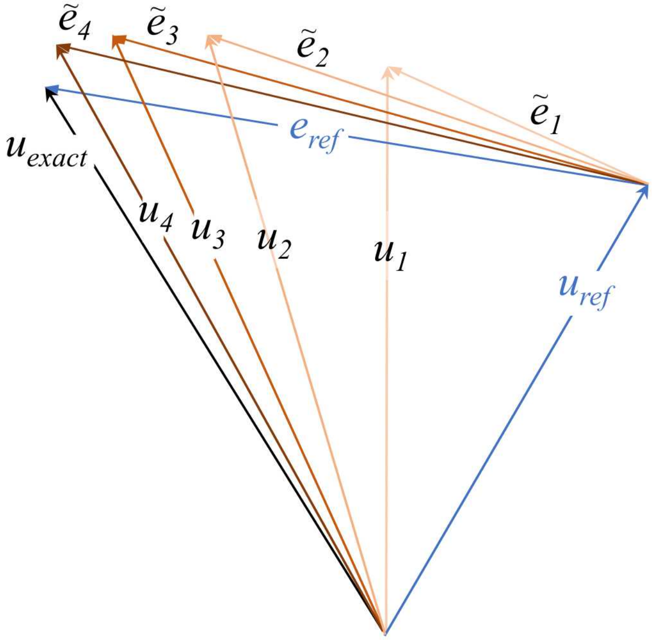

*Figure 7. Initial apparent divergence from an inexact reference solution but with monotonic convergence to a fixed apparent error.*

The final case examined here (Figure 7) can occur when the error in the reference solution is so large that even the coarsest meshes suggests a lack of convergence, when in reality the numerical solution is converging to the exact solution. In this case there is no indication of convergence as the error continues to grow to a fixed value. This is a subset of the above case, in the sense that if mesh 5 in the previous case had been the coarsest mesh, the convergence response would be the same as this case. This highlights an important point: that the cases we are presenting are defined not just by the magnitude of the error in the reference solution but also by the mesh sequence adopted for the convergence study. That is, it is the relative size (and orientation) of the error in the reference solution compared to the errors in the numerical solutions that affects whether we can at least observe a convergence trend for the coarsest meshes. Whether this convergence is asymptotic or not still depends upon the magnitude of the higher order terms.

In the next section we present a model stress concentration problem, its classical solution, and a manufactured (exact) solution that are the subject of the numerical study presented in Section 4. In the later section, we present convergence plots that correspond to several of the cases presented above. We will see cases in which the numerical solutions with an exact reference solution yield the expected asymptotic response, and when using an inexact reference solution they (a) diverge, (b) show non-asymptotic convergence initially and then converge to a fixed error, and (c) exhibit asymptotic response until the errors in the numerical solution become smaller and $e_{ref}$ becomes too large for the surrogate reference solution to be useful.

# 3. STRESS CONCENTRATION MODEL PROBLEM – ANALYTICAL SOLUTIONS AND MODELS

A stress concentration model problem, adapted from a brief study [Orient and Alvis 2017], was examined to determine why convergence was not apparent in the initial results. The initial results were based upon a linear elastic solution, and yet the code approximates the fully-nonlinear equations of motion. Parameter studies had been conducted to examine the effect of different model parameters and modeling assumptions, but the scope of the study precluded a detailed examination.*

## 3.1. Classical Infinite Domain Stress Concentration Problem

The classical stress concentration problem for a hole in an infinite plate is schematically represented in Figure 8. It has elastic properties typical of steel, and plane strain conditions are applied to the plate. The edge tractions correspond to the far-field values, and the magnitude of 3000 psi represents the value used in the initial study. For some analyses the traction value was increased beyond this value. The physical behavior was assumed to be governed by the equations of linear elasticity.

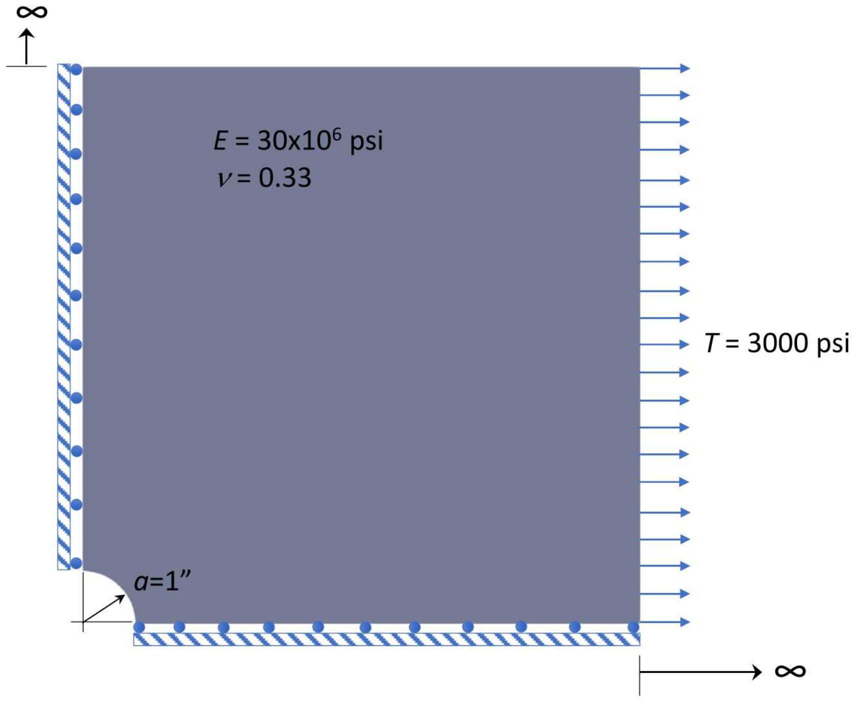

*Figure 8. Stress concentration problem – hole in an infinite plate.*

---

* Note that these are not negative comments about the initial study but rather reflect the dilemma often faced when using an inexact reference solution but having limited time in which to examine all the factors that may be affecting the apparent lack of convergence. The contact convergence tests in the Sierra/SM fall into this same category; convergence was not apparent using the selected meshes unless one resorted to Richard Extrapolation to demonstrate a tendency to converge to some solution.

### 3.2. Classical Solution for the Stress Concentration Problem

The solution for this problem is presented in many text books (*ref. e.g.*, Muskelishvili [1953] and Sokolnikoff [1956]) and is obtained from complex analyses based upon Airy's stress function. The solution is initially obtained in polar coordinates and then transformed to give the displacement field components in rectangular Cartesian coordinates as

$$u_x = \frac{T}{8\mu}\left[\frac{(\kappa+1)r^2\left(2a^2+r^2\right)\cos(\theta)+2a^2\left(r^2-a^2\right)\cos(3\theta)}{r^3}\right]$$

$$u_y = \frac{Ta}{8\mu}\left(-\frac{2a^3\sin(3\theta)}{r^3}+\frac{2a(-\kappa\sin(\theta)+\sin(\theta)+\sin(3\theta))}{r}+\frac{(\kappa-3)r\sin(\theta)}{a}\right) \qquad (16a,b)$$

where $(r, \theta)$ denote the polar coordinates, $\mu$ denotes the shear modulus, $\nu$ denotes Poisson's ratio, for plane strain $\kappa = 3\text{-}4\nu$, and $T$ and $a$ are depicted in Figure 8.

Applying the strain-displacement and constitutive relationships, the non-zero stress tensor components are then given by

$$\sigma_{xx} = T\left[1-\frac{a^2}{r^2}\left(\frac{3}{2}\cos(2\theta)+\cos(4\theta)\right)+\frac{3a^4}{2r^4}\cos(4\theta)\right] \qquad (17a\text{-}d)$$

$$\sigma_{yy} = T\left[-\frac{a^2}{r^2}\left(\frac{1}{2}\cos(2\theta)-\cos(4\theta)\right)-\frac{3a^4}{2r^4}\cos(4\theta)\right]$$

$$\sigma_{xy} = T\left[-\frac{a^2}{r^2}\left(\frac{1}{2}\sin(2\theta)+\sin(4\theta)\right)+\frac{3a^4}{2r^4}\sin(4\theta)\right]$$

$$\sigma_{zz} = T\nu\left[1-\frac{2a^2}{r^2}\cos(2\theta)\right]$$

The solution above is referred to as the *classical reference solution* in the next section. While it has an appeal in its relative simplicity, the convergence response based upon using it as the reference solution can appear more complex than when using the more complex manufactured solution presented in the next subsection.

### 3.3. Manufactured Solution for the Stress Concentration Problem

As previously discussed [Cox 2016], when "manufacturing a solution," we really are manufacturing a problem that our solution solves. In this case, we start with the displacement field given by Equations (16). As such both reference solutions share this field, but their stress responses and boundary value problems will differ; the differences of which will increase with the load level. The original differences in the boundary value problem include a nonlinear (quadratic) strain displacement relationship (*vs*. linear), and equilibrium is enforced in the deformed configuration (*vs*. the undeformed configuration). An outline of the nonlinear equations used in the manufacturing is given by Cox [2016], and the linear elasticity equations are available in classic texts (*e.g.*, Skolnikoff [1956]). We follow the manufacturing procedure discussed in Cox [2016] in which the governing equations are applied to the displacement field to obtain strain measures, stress measures, boundary tractions (where needed), and then body loads. In contrast, the original problem did not even have body loads. In this context they can be thought of as a necessary change to the problem description to yield the displacements from a linear elastic solution when the problem is completely out of the linear elastic regime. In other words, the body loads grow to offset the nonlinearities that would in their absence give a different displacement response.*

In presenting the manufactured solution, only a subset of the derived relationships are presented, mainly as an act of kindness to the reader. The actual relationships were obtained using the Hyperelastic Factory [Cox 2013, 2016], a Mathematica "program." Mathematica is designed for complex expressions; we are not, but presenting selected relationships conveys the complexity that develops during the "manufacturing." Most of the expressions were obtained directly from Mathematica, letting it convert them to LaTeX after having it fully-simplify them. Later expressions in the manufacturing process became too complex even with automatic conversion to LaTeX to be typeset, so I have "punted" and present the Mathematica results directly in Appendix I.

Let $\phi$ denote the motion (or configuration) map between the initial ($\mathbf{X}$) and current ($\mathbf{x}$) configurations, given by

$$\boldsymbol{x} = \phi(\boldsymbol{X}, t) \tag{17}$$

where *t* denotes time. In terms of the displacements given by Equations (16), we can write

$$\phi(\boldsymbol{X}, t) = \boldsymbol{X} + \boldsymbol{u}(\boldsymbol{X}, t) \tag{18}$$

where the traction, *T,* implicitly provides the time variation.

The manufacturing process starts with obtaining the deformation gradient, **F**, from the displacement field as

$$\boldsymbol{F} = \nabla_0 \phi = \boldsymbol{I} + \nabla_0 \boldsymbol{u} \tag{19}$$

where $\nabla_0$ is the material gradient operator, and ***I*** is the second order identity tensor. The nonzero components of the tensor are given by

$$F_{11} = \frac{\frac{2a^2T\left(-X_2^2X_1^2\left(18a^2+(\kappa-10)X_1^2\right)+X_2^4\left(3a^2+(\kappa+10)X_1^2\right)+3a^2X_1^4-(\kappa+2)X_1^6+(\kappa-2)X_2^6\right)}{\left(X_1^2+X_2^2\right)^4}+8\mu+\kappa T+T}{8\mu}$$

---

[*] It is interesting to note that some early forms of boundary integral equation methods (BIEMs) or boundary element methods (BEMs), body loads were used somewhat conversely. That is, in that context the Greens functions (upon which the BEMs were derived with) were inherently for linear elastic problems. To obtain nonlinear responses fictitious body loads were introduced to extend the methods beyond a linear elastic response, not to constrain it to be like a linear elastic response.

$$F_{12} = \frac{a^2 T X_1 X_2 \left(-2X_2^2 \left(3a^2 + (\kappa+2)X_1^2\right) + 6a^2 X_1^2 - (\kappa+6)X_1^4 - (\kappa-2)X_2^4\right)}{2\mu \left(X_1^2 + X_2^2\right)^4}$$

$$F_{21} = \frac{a^2 T X_1 X_2 \left(2X_1^2 \left(3a^2 + \kappa X_2^2\right) - 6a^2 X_2^2 + (\kappa-4)X_1^4 + (\kappa+4)X_2^4\right)}{2\mu \left(X_1^2 + X_2^2\right)^4} \tag{20a-e}$$

$$F_{22} = \frac{-\frac{2a^2T\left(X_1^4\left(3a^2+(\kappa+8)X_2^2\right)-X_1^2\left(18a^2X_2^2+(\kappa-12)X_2^4\right)+3a^2X_2^4+(\kappa-4)X_1^6-\kappa X_2^6\right)}{\left(X_1^2+X_2^2\right)^4} + 8\mu + (\kappa-3)T}{8\mu}$$

$$F_{33} = 1$$

We also need the Jacobian for conversion between stress measures, which is given by

$$\begin{aligned} J \;=\; & [4X_1^6(a^2T((5-(\kappa-2)\kappa)T - 8(\kappa-1)\mu) + X_2^2(8\mu + (\kappa-3)T)(8\mu + \kappa T + T)) \\ & +2X_1^4(2a^4((\kappa-2)\kappa - 14)T^2 - 2a^2TX_2^2(8(\kappa-1)\mu + ((\kappa-2)\kappa \\ & +19)T) + 3X_2^4(8\mu + (\kappa-3)T)(8\mu + \kappa T + T)) - (6a^4T - 2a^2\kappa TX_2^2 - X_2^4 \\ & (8\mu + (\kappa-3)T))(6a^4T + 2a^2(\kappa-2)TX_2^2 + X_2^4(8\mu + \kappa T + T)) + 4X_1^2 \\ & (18a^6T^2 + 2a^4(\kappa(\kappa+6) + 14)T^2X_2^2 + a^2TX_2^4(8(\kappa-1)\mu + ((\kappa-2)\kappa - 21) \\ & T) + X_2^6(8\mu + (\kappa-3)T)(8\mu + \kappa T + T)) + X_1^8(8\mu + (\kappa-3)T)(8\mu + \kappa T + T)]/ \\ & \left[64\mu^2\left(X_1^2 + X_2^2\right)^4\right] \end{aligned} \tag{21}$$

After obtaining the Lagrangian or Green strains (**E**), the second Piola-Kirchhoff stress (**S**) is obtained from the St. Venant-Kirchhoff constitutive relationship given by [*ref. e.g.*, Bonet and Wood 2008]

$$\boldsymbol{S} = \lambda(tr\boldsymbol{E}) + 2\mu\boldsymbol{E} \tag{22}$$

For illustrative purposes, two representative normal and shear stress components of the second Piola-Kirchhoff stress are given by

$$\begin{aligned} S_{11} = & \frac{1}{64\mu}\Bigg[\Bigg(\frac{2a^2T\left(-X_2^2X_1^2\left(18a^2 + (\kappa-10)X_1^2\right) + X_2^4\left(3a^2 + (\kappa+10)X_1^2\right) + 3a^2X_1^4 - (\kappa+2)X_1^6 + (\kappa-2)X_2^6\right.}{\left(X_1^2 + X_2^2\right)^4} \\ + & \quad \frac{8\mu + \kappa T + T}{\left(X_1^2 + X_2^2\right)^4}\Bigg)^2 + \frac{16a^4T^2X_1^2X_2^2\left(2X_1^2\left(3a^2 + \kappa X_2^2\right) - 6a^2X_2^2 + (\kappa-4)X_1^4 + (\kappa+4)X_2^4\right)^2}{\left(X_1^2 + X_2^2\right)^8} - 64\mu^2\Bigg] \\ + & \quad \frac{\lambda T}{64\mu^2}\Bigg[\frac{4a^2(8(\kappa-1)\mu + ((\kappa-2)\kappa - 1)T)}{X_1^2 + X_2^2} + \frac{4a^4((\kappa-2)\kappa + 8)T - 8a^2X_1^2(8(\kappa-1)\mu + ((\kappa-2)\kappa - 13)T}{\left(X_1^2 + X_2^2\right)^2} \\ + & \quad \frac{4a^4T\left(9a^4 - 12a^2X_1^2 - 16(\kappa-3)X_1^4\right)}{\left(X_1^2 + X_2^2\right)^4} + \frac{8a^2T\left(-3a^4 + 4a^2(2\kappa-5)X_1^2 - 16X_1^4\right)}{\left(X_1^2 + X_2^2\right)^3} \\ + & \quad 16\kappa\mu - 16\mu + \kappa^2T - 2\kappa T + 5T\Bigg] \end{aligned} \tag{23a,b}$$

$$
\begin{aligned}
S_{12} = {} & \frac{a^2 T X_1 X_2}{8\mu (X_1^2 + X_2^2)^6} \Big[ 6a^4(1-3\kappa)T X_2^4 + 2X_1^6 \Big( a^2(24\mu + 11\kappa T - 5T) + 2X_2^2(-24\mu - 5\kappa T + T) \Big) \\
+ {} & 2a^2 X_2^6(-24\mu + \kappa T + T) + 6X_1^4 \Big( a^4(1-3\kappa)T + a^2 X_2^2 \big(8\mu - 3(\kappa+1)T\big) - X_2^4(8\mu + 3\kappa T + T) \Big) \\
+ {} & 2X_2^2 X_1^2 \Big( 6a^4(5\kappa+1)T - a^2 X_2^2(24\mu + 19\kappa T + 3T) - 2X_2^4\big((\kappa+3)T - 8\mu\big) \Big) + X_1^8\big((3-7\kappa)T - 40\mu\big) \\
+ {} & X_2^8\big(24\mu + (\kappa-5)T\big) \Big]
\end{aligned}
$$

The Cauchy stress (**σ**) is then obtained using the Piola transformation combined with volume scaling as

$$\boldsymbol{\sigma} = J^{-1} \boldsymbol{F} \boldsymbol{S} \boldsymbol{F}^T \tag{24}$$

For brevity, we have not presented the components of the Cauchy stress "in full glory" in the main text, for the sake of the reader (and the type-setter), however Mathematica results for the stress components are given in Appendix I. Generally the complexity continues to increase with each step of the symbolic manipulations. The C code generated by Mathematica for $\sigma_{11}$, which is pasted into the SM and Encore input files, was 89 lines.

Assuming quasi-static conditions as the initial classical solution, the body loads ($\mathbf{f_0}$) in the reference configuration can be obtained from the divergence (with respect to the reference configuration) of the first Piola-Kirchhoff, or from the divergence (with respect to the spatial configuration) of the Cauchy stress combined with a volume scaling. The later relationship is given by

$$\boldsymbol{f}_0 = -J div(\boldsymbol{\sigma}) \tag{25}$$

Again we omit the expressions for the body loads due to their complexity, but the two nonzero body load components, as given by Mathematica, are also listed in Appendix I. These expressions are also output by Mathematica in C code form, and then pasted into the SM input file as body load functions.

The increase in complexity with the expressions for stresses versus those from linear elasticity (Equations (**Error! Reference source not found.**)) and the existence of the complex body loads for the manufactured solution make it obvious why we would prefer to use linear elastic solutions for at least some of the testing. However, as discussed in Section 2 and demonstrated in Section 4, while the solutions are simpler the interpretation of the verification results when using them is not.

Automating the manufacturing of solutions using symbolic manipulation directly in the analysis code has been addressed at Sandia and other institutions. While doing so eliminates the manual steps mentioned above and thus improves the efficiency of code verification, examination of the intermediate steps has sometimes provided insight to the limitations of the verification problems [Cox 2016]. Furthermore, the automated approach has its limitations once history dependence is included in the problem, since the strong form contains integrodifferential equations and thus automatic differentiation is no longer sufficient to automate the process.

## 3.4. Mathematical and Computational Models

In this subsection we consider a few variations of the mathematical and computational models. For the mathematical models we consider differing boundary conditions, and for the computational models we consider different meshes. The initial approximation made in the modeling is replacing the infinite domain of the original mathematical model with a finite domain, as depicted below. This model matches the one used in the preliminary study on the problem. Each of these mathematical models will be labeled as *Classical model case n*, indicating the corresponding reference solution for model *n* is the classical linear elasticity solution. While we associate the equations of linear elasticity with the mathematical model, the actual governing equations upon which the code is based are nonlinear; we can only seek the classical solution in the limit of infinitesimal loading.

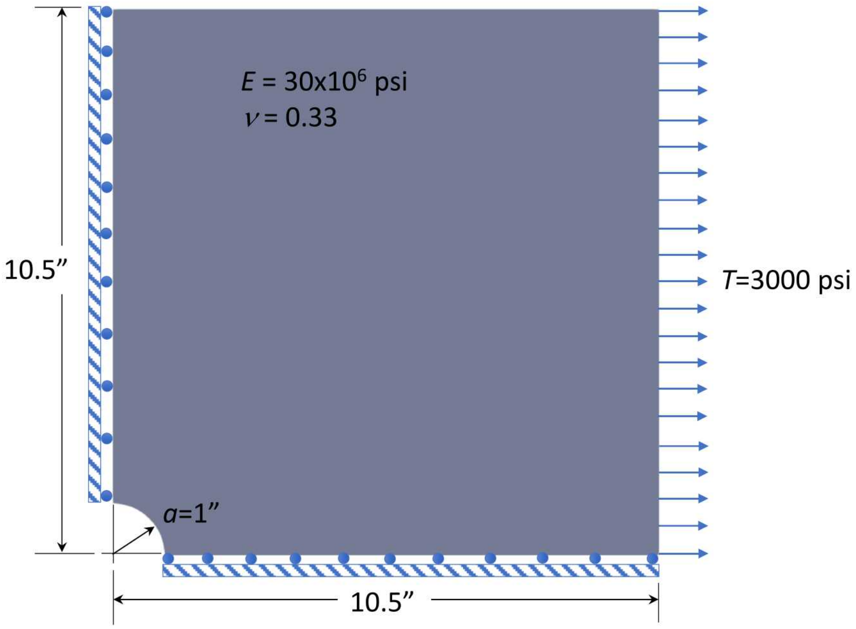

*Figure 9. Classical model case 1: finite domain model used for first analyses with a classic reference solution.*

### 3.4.1. Mesh Discretizations

Two sequences of mesh discretizations were considered in the convergence studies; the first three meshes of each sequence are depicted in Figure 1. Each successive mesh in the sequence is obtained from uniform mesh refinement of its "coarser neighbor," but nodes on the finer meshes do conform to the actual geometry. Each element is divided into 4, 2 in each in-plane local coordinate direction. Mesh sequence *A* was the sequence used in the original preliminary study of the problem. Based upon engineering knowledge of the problem, it is more concentrated near the top of the hole to better resolve the stress concentration (a higher mesh density by a factor of about 3). Mesh sequence *B* was examined as a coarser mesh sequence to see if it might affect the convergence behavior. Since Sierra/SM is a three-dimensional code, plane strain is modeled by constraining displacements normal to the plane of a single-element-thick sheet of three-dimensional elements. The thickness of the sheet is approximately equal to the in-plane dimension of the element adjacent to the top of the circle (where the stress concentration is maximum). While this implies rather extreme aspect ratios will occur in other parts of the mesh, verification testing for Sierra/SM has shown aspect ratios calculated from element dimensions in directions of zero gradient do not affect the accuracy of the results. Nearly all of the results presented in the next section were based upon mesh sequence $A$; mesh $B$ was merely used to show invariance of the convergence results with respect to the mesh sequence when using a classical reference solution, and to see if a coarser base mesh might be able to represent more of the ideal convergence response depicted in Figure 2.

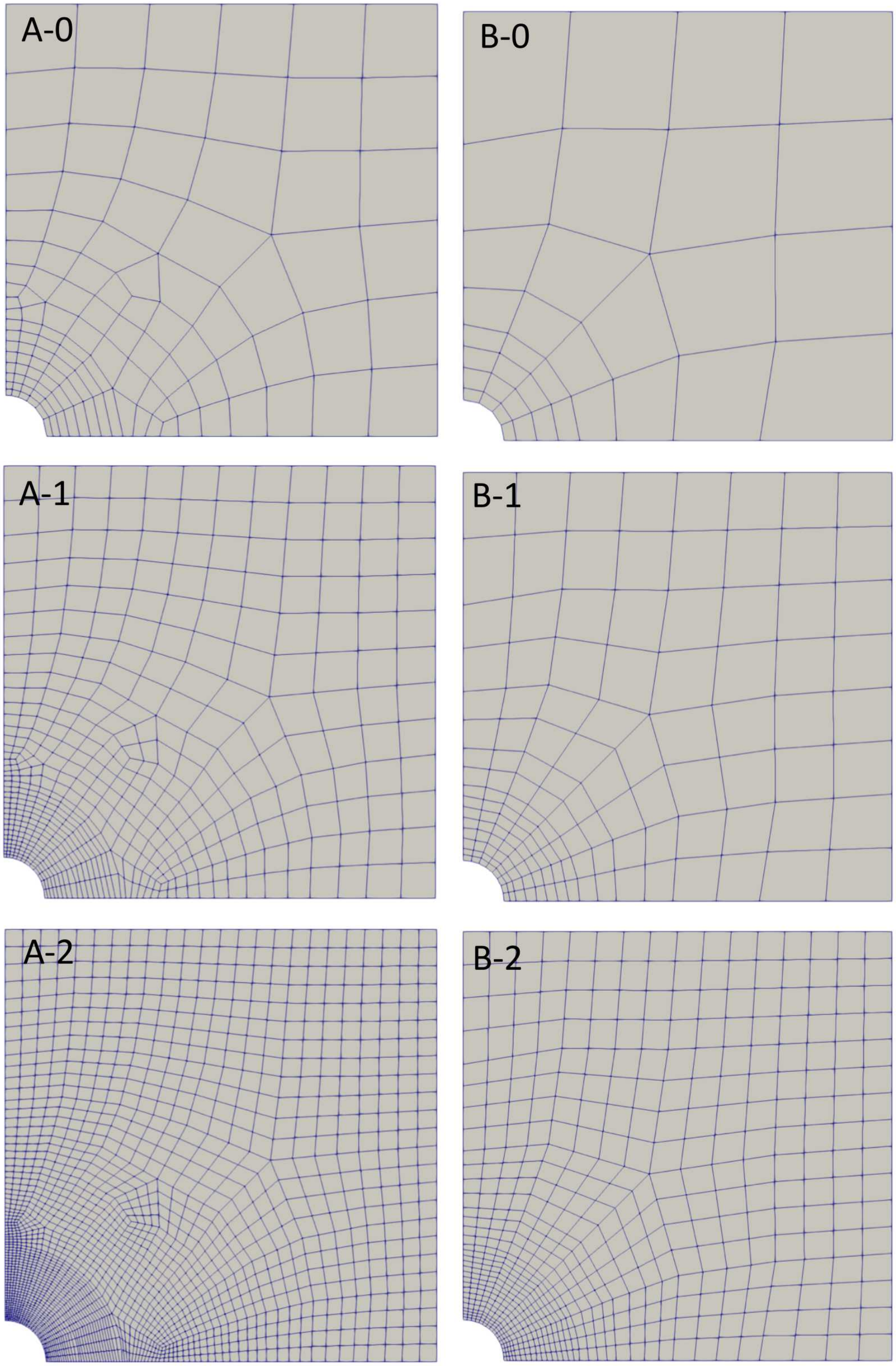

*Figure 10. Mesh sequences – first three meshes of the two mesh sequences considered in the convergence studies. A ~ the original mesh sequence with finer density near the point of greatest stress concentration. B ~ less concentrated mesh sequence (for quicker convergence studies).*

### 3.4.2. Boundary Conditions

To examine the effect of the finite domain approximation and the corresponding boundary conditions, two other boundary conditions cases were considered. Note that these were only used when comparing numerical results to the classical reference solution. The first (case 2), depicted in Figure 11, eliminates the errors associated with the finite domain approximation by applying the displacement values from Equations (16) to the far boundaries of the domain, instead of applying the far field stress states. The displacement vectors are sketched with ball-headed arrows merely to depict relative orientations (not accurately scaled).

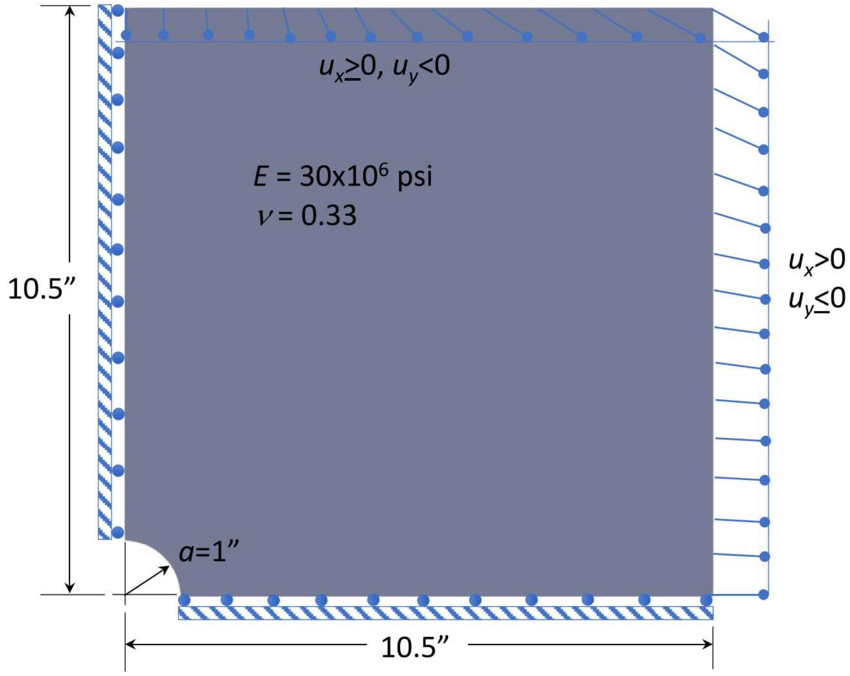

*Figure 11. Classical model case 2: finite domain model used for analyses with a classic reference solution – analytical displacements applied to outer boundary surface.*

The second modification (case 3) of the original mathematical model (case 1, Figure 9) applied the displacement values from Equations (16) to all boundaries of the domain as depicted in Figure 12. Note that case 3 corresponds to the boundary conditions selected for the manufactured solution, but it does not fully represent the boundary value problem used in that case, as the problem for the manufactured solution has a spatially varying body load over the full domain.

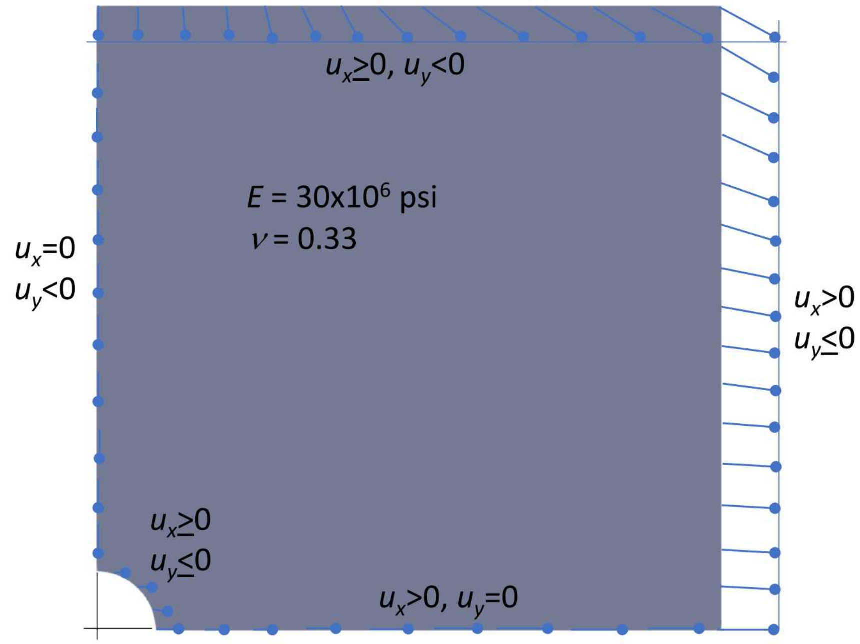

*Figure 12. Classical model case 3: finite domain model used for analyses with a classic reference solution – analytical displacements applied to all surfaces.*

# 4. VERIFICATION RESULTS

This section presents the results of the verification analyses using both the classical and manufactured reference solutions discussed in the previous section. As explained in our previous verification studies [Cox and Mish 2013], the $L_2$-norm used is for a Voight representation of the stress tensor components (*i.e.*, a vector form), consistent with the Exodus file storage scheme. This "vector" form constitutes an equivalent norm to the standard tensor norm. Note that we will refer to the differences between the numerical results and the reference solutions, consistently as the *error* (or *relative error*), independent of the reference solution, knowing full well that for the case of the classical reference solution it is the *apparent error* not the *true error* (*ref.* Section 2).

## 4.1. Comparison using Classical Reference Solutions with Different Meshes

First we consider results using a classical reference solution and using the boundary conditions of case 1 for the numerical solution (*i.e.*, the basis for the preliminary study). Figure 13 shows stress convergence results using mesh sequences *A* and *B*. Note that $h_0$ corresponds to the coarsest (base) mesh for each sequence. Since the meshes are not uniform, the element size is normalized by $h_0$, such that, *e.g.*, $h_1/h_0=1/2$, implying that the element sizes are halved throughout the nonuniform mesh. Mesh *A-0* is about 1/3 as fine as mesh *B-0* (based upon the element size near the top of the circle, highest stress concentration point), and as such the relative errors are consistently smaller for mesh sequence *A*. As a sanity check, both mesh sequences appear to converge to the same relative error.

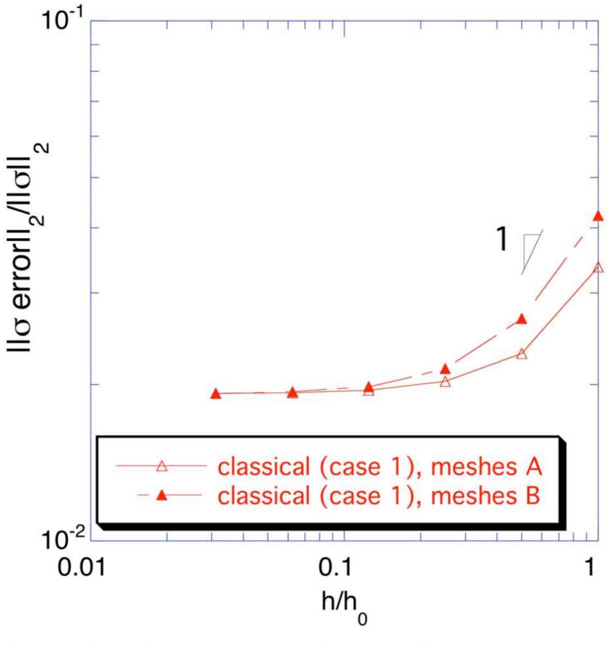

*Figure 13. Comparison of stress divergence results for two mesh sequences based upon a classical reference solution (model case 1).*

The coarsest meshes are apparently the closest to being the asymptotic range with convergence rates of approximately 0.55 and 0.66 for mesh sequences *A* and *B*, respectively. While the engineering judgement that led to mesh sequence *A* provided improved accuracy (relative to *B*), the finer mesh made it slightly more difficult to estimate the convergence rate. Coarsening the mesh sequence helps some because the coarser-mesh numerical solutions are made to be further from both the classical reference solution and exact solution; thus making the apparent error closer in size to the true error (*ref.* Figure 4). However, neither mesh sequence provided an accurate approximation of the asymptotic rate of 1. With further mesh refinement the results are clearly in the *inaccurate reference range* (*ref.* Figure 2) for both mesh sequences. From this point onward, we only consider results for mesh sequence *A*.

## 4.2. Improving the Classical Reference Solution Results

The natural question asked after the preliminary study (and that has been previously asked about several Sierra/SM tests) was "why can we not measure the rate of convergence when using the classical reference solution in this case?" Followed by "does this imply something is wrong with the code?" To answer the second question, we manufactured a solution to the related problem that was consistent with the nonlinear governing equations that the code approximated (*ref.* Section 3.3).

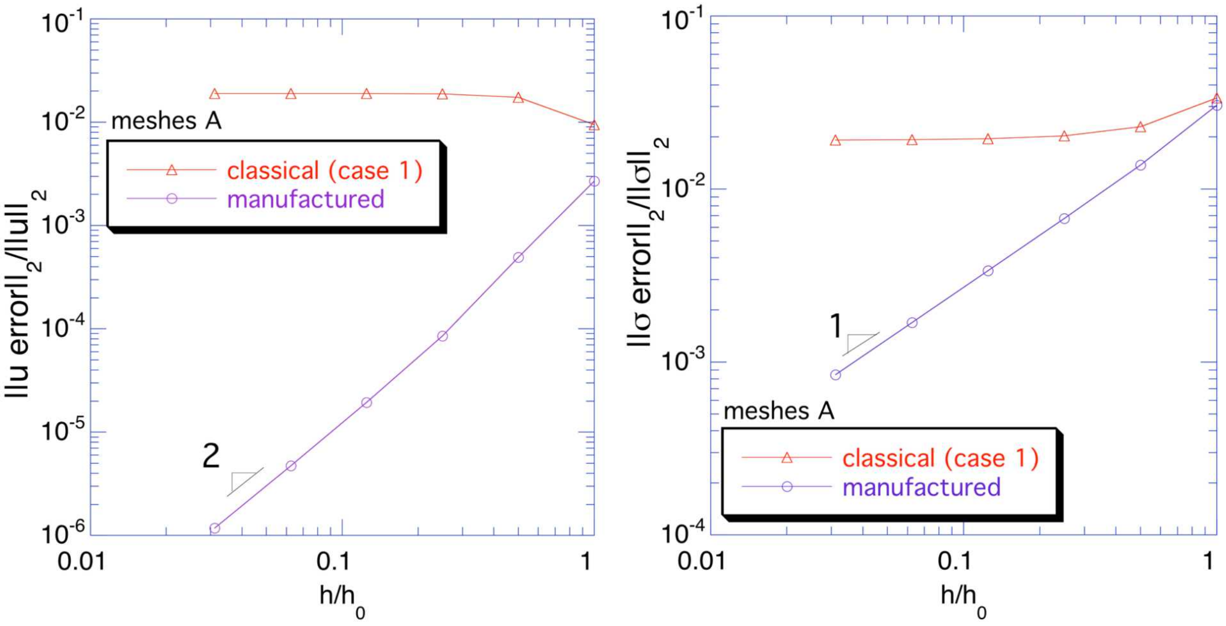

*(a) Displacements* *(b) Stresses*

*Figure 14. Convergence to the manufactured solution versus the classical solution – case 1.*

(a) Displacements (b) Stresses

Figure 14 shows the convergence results for both the displacement and stress fields, comparing results obtained with the initial classical and manufactured reference solutions. Of course not only are the reference solutions different, but so are the mathematical models. Note that the divergence of the displacements with the classical reference solution shows an increase in the error converging to a fixed error value, as Figure 7 represented.

These results answer the question about a possible code error, since with the manufactured solution (an exact reference solution) the code accurately reproduces the expected asymptotic rates of convergence for displacements (2.005), and stresses (1.0005).

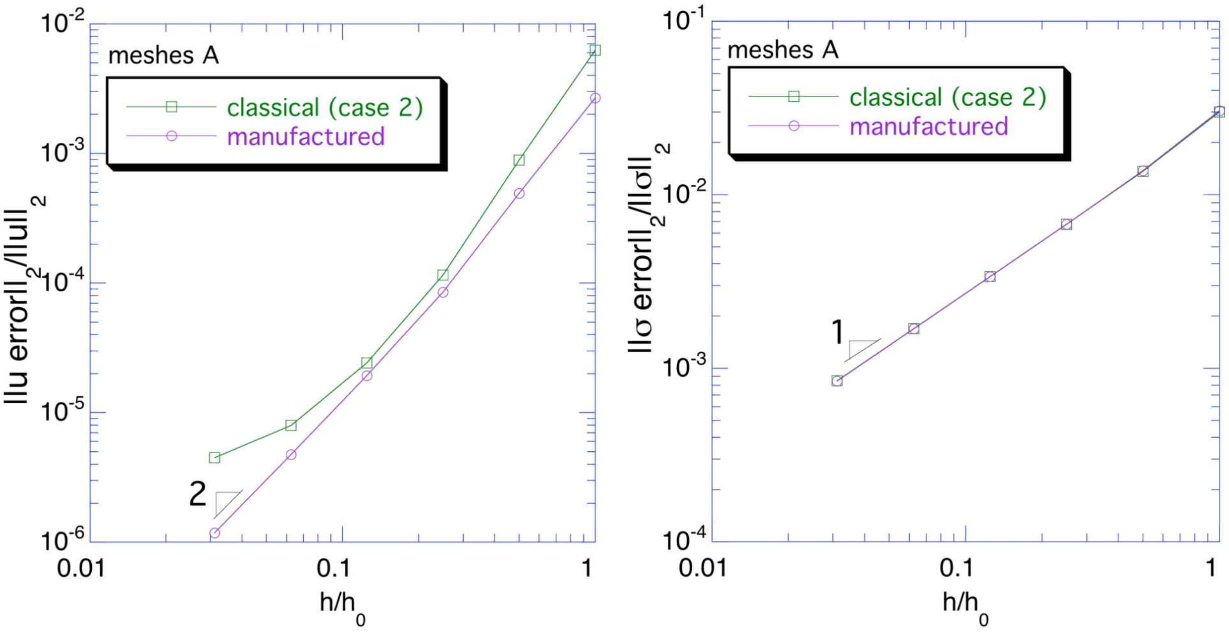

*(a) Displacements* *(b) Stresses*

*Figure 15. Convergence to the manufactured solution versus the classical solution – case 2.*

To answer the question as to why we could not get the classical reference solution to yield an approximation to the asymptotic rates, we examine the effects of changing the boundary conditions to be closer to those used in the manufactured solution. In effect we shift the exact solution closer to the inexact reference solution (Figure 4 versus Figure 5).

Figure 15 shows the convergence results for both the displacement and stress fields, comparing results obtained with the classical (case 2) and manufactured solutions. By changing from the far-field traction conditions to displacements at the actual edge of the specimen (Figure 11) the results improve significantly. For the convergence of the displacement field, one could argue that all three regions of Figure 2 are exhibited, though the meshes for which the asymptotic rate are exhibited is only known by comparing with the manufactured solution result (*i.e.*, by itself the classical reference does not give strong evidence of attaining the asymptotic rate of convergence). The stress field on the other hand does yield strong evidence of attaining the asymptotic rate of convergence; in fact, graphically the results for the manufactured and classical reference solutions are indistinguishable. This trend of the classical solution serving as a better reference solution of the stresses ($O(1)$) than the displacements ($O(2)$) will generally occur with a displacement-based FE formulation, since the errors for the displacements will tend to be much smaller and thus much more sensitive to errors in the reference solution.[*]

---

[*] For a much more complete discussion of this trend reference Cox and Mish [2013].

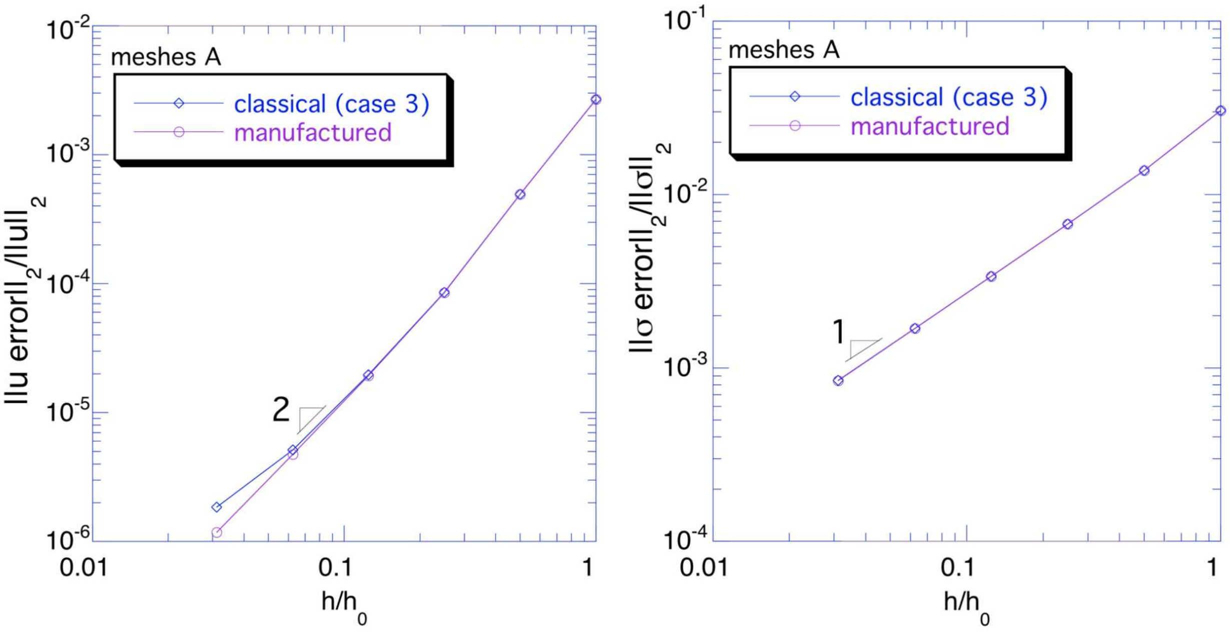

*(a) Displacements* *(b) Stresses*

*Figure 16. Convergence to the manufactured solution versus the classical solution – case 3.*

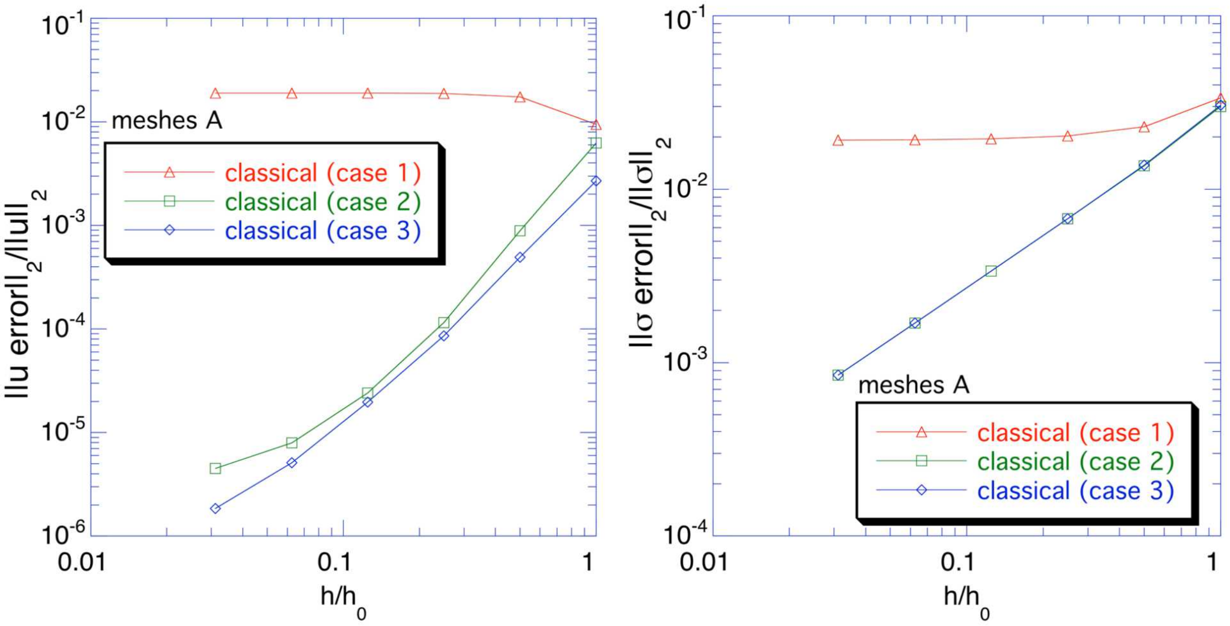

*(a) Displacements* *(b) Stresses*

*Figure 17. Comparison of the convergence of all three classical solution numerical models for the displacement and stress fields.*

Finally let’s examine the convergence results for the classical (case 3) and manufactured solutions. Figure 16 shows the convergence results for both the displacements and stress fields. By changing all of the boundary conditions to the known displacements (Figure 12) the displacement results show further improvement. Unlike the previous two mathematical models for the classical solution, this one clearly reveals the asymptotic rate of convergence for both response fields. It is only for the finest mesh that the displacement field starts to exhibit behavior characteristic of the *inaccurate reference range*.

Figure 17 shows the progression of improved convergence results as the boundary conditions change from the simplest approximation of the classical problem to one that shares the boundary conditions of the manufactured solution (but not the body loads). The results certainly suggest that for the selected finite domain size the far-field traction boundary conditions were not adequate for a convergence study.

A typical quantity of interest in this problem is the magnitude of the stress concentration (3), *i.e.*, the ratio of the maximum stress to that of the far-field value. The highest stress concentration is at the top of the circular hole, and for each analysis the maximum stress value occurred at the element closest to the top of the circular hole. Figure 18 depicts the convergence of the maximum stress value for the three models. Model case 1 appears to yield a non-monotonic convergence to a fixed error (*ref*. Figure 6), and the other two cases exhibit linear asymptotic convergence, consistent with the asymptotic convergence rate for the entire field.

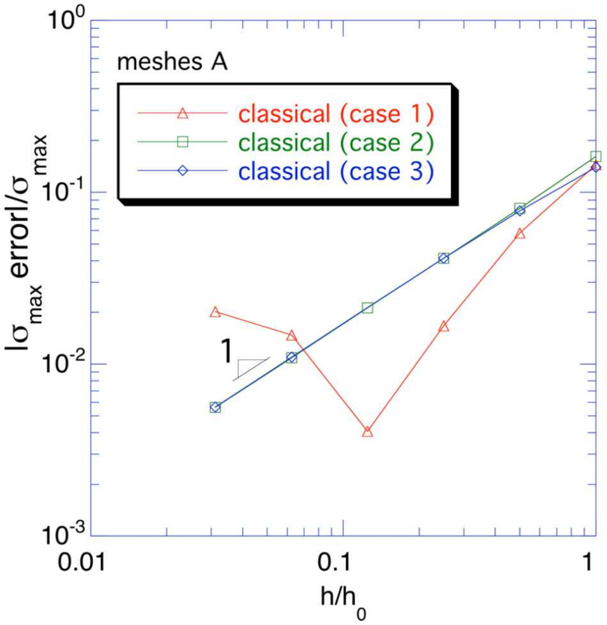

*Figure 18. Comparison of the convergence of all three classical solution computational models for the maximum stress.*

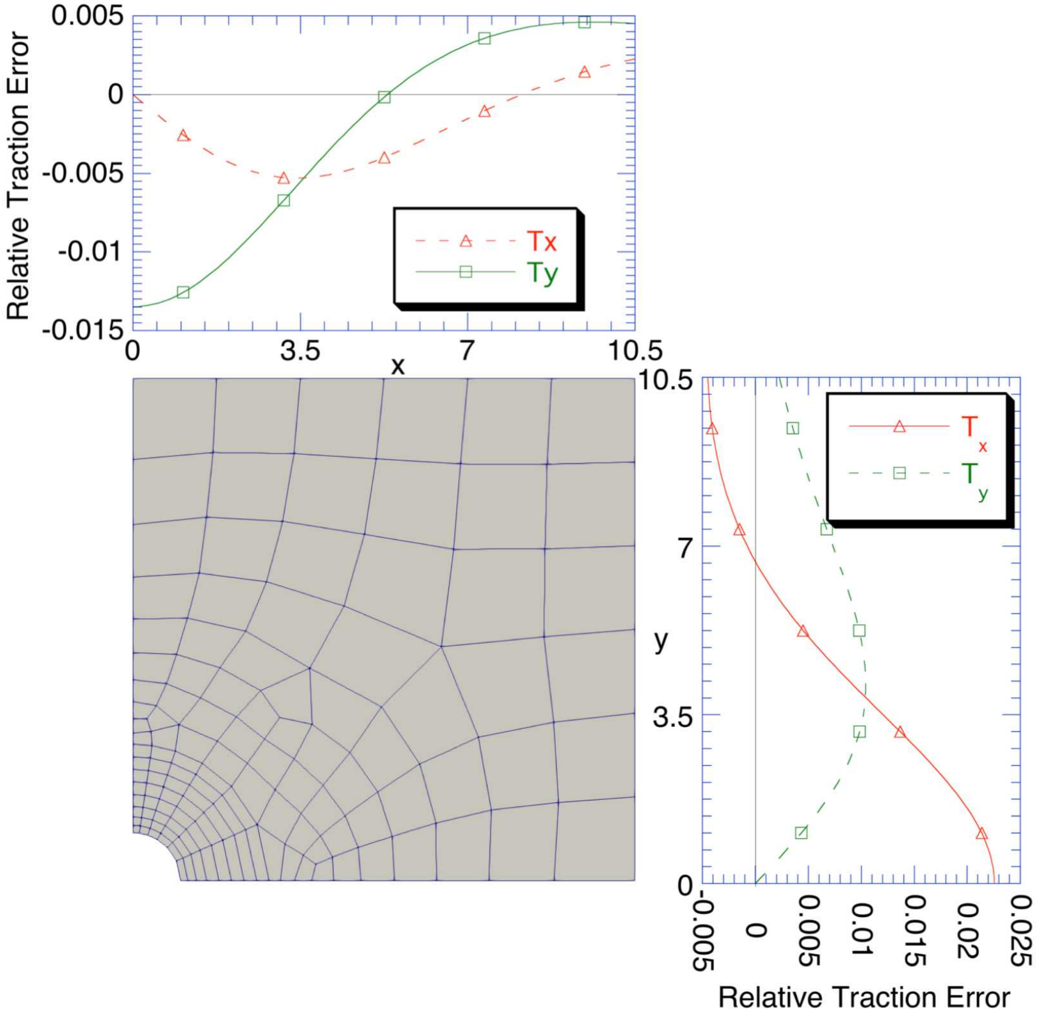

*Figure 19. Traction errors when adopting the far-field values for the finite domain. (Depicted with mesh A-0 merely to show the edges the tractions occur on.)*

To confirm that the adoption of the far-field traction boundary conditions was the main cause for the lack of convergence with the case 1 model, we use the stress field in the classical analytical solution, Equations (17), to determine the theoretical tractions on the edge of the finite domain. Figure 19 shows the errors in each prescribed traction component on the domain's outer edges due to adopting the far-field values. The maximum error in the traction is about 2.25% and occurs on the vertical edge. This boundary condition error dominates the error norm of the fields making the effect of the discretization error unmeasurable, and yielding nominally 2 percent errors in both fields. Note that in leu of prescribing displacement boundary conditions (classical model cases 2 and 3), one could have increased the size of the domain until the error in adopting the far field traction was sufficiently small. Unfortunately that approach would require a much larger domain, since very accurate traction values would be required to not "cover up" the relatively small discretization errors that occur with the finer meshes. Alternatively one could have applied the tractions obtained from the analytical solution (as used above to calculate the error in applying the far field values), instead of the displacements, to the edges of the existing meshes. Of course applying the calculated displacements or tractions has some of the nature of a manufactured solution, because we had to know the solution to determine the boundary conditions.

### 4.3. Failure of the Classical Reference Solution with Increased Loading

As noted above, even with the improved boundary conditions (model case 3), for the finest mesh the displacement field error appears to be starting to exhibit errors characteristic of the *inaccurate reference range* (*ref.* Figure 16). As such, we would expect with further mesh refinement that the error would approach the error in the reference solution (*ref.* Figure 2).

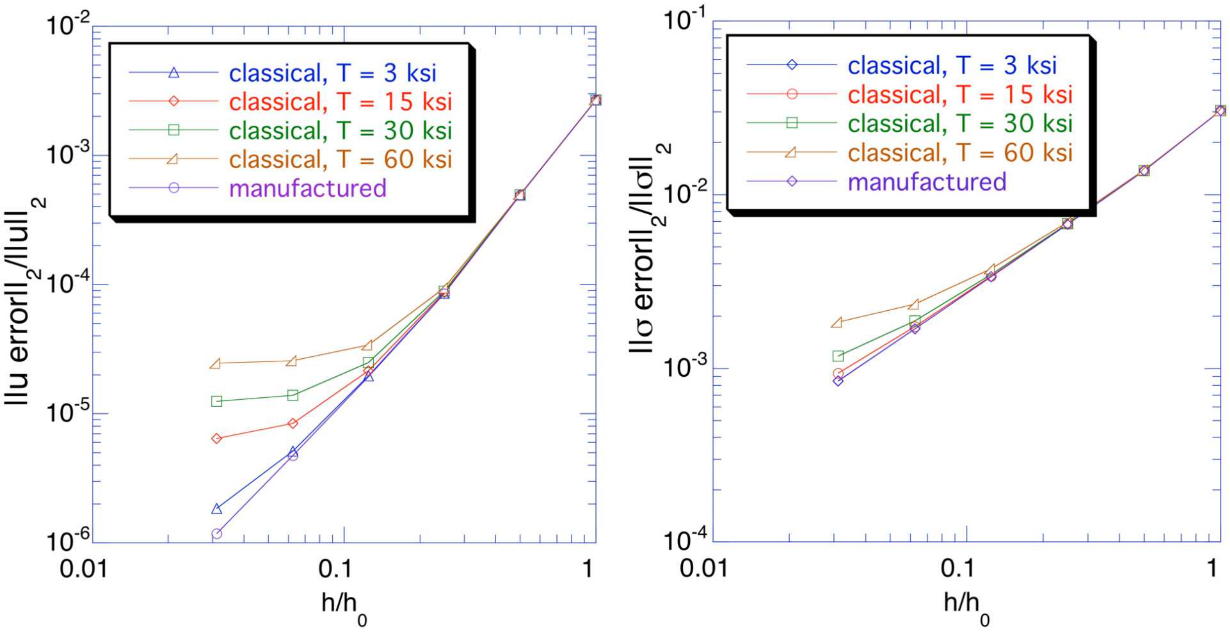

*(a) Displacements* *(b) Stresses*

*Figure 20. Increased inaccuracy of the classical reference solution with increased loading levels.*

From a mechanics point of view, we would also expect that as we increased the load level the nonlinearities in the equations that govern the code would become more important, and thus the results would deviate more from the classical solution. For example, the second order terms in the strain-displacement relationship would become more significant and would deviate from the linear strain-displacement relationship assumed in linear elasticity.

Figure 20 depicts results that follow from increasing the load from the previous level (3 ksi) to as much as 20x higher (classical model 3). The expected trends with increasing load are: (1) the apparent error increases, (2) more of the convergence response is in the inaccurate reference range and less in the asymptotic range, and (3) the deviations from the convergence response with an exact reference solution occurs at lower load levels with displacements than with stresses (which follows from the greater accuracy of the displacements [Cox and Mish 2013]).

Relating this trend back to discussion in Section 2, increasing the load level increases the distance between the inexact reference solution and the exact solution. This corresponds to the increased apparent error ($e_{ref}$) and also explains why only increasingly coarser meshes (those further from the exact solution) would still be within the asymptotic range. Of course if the load were increased enough, an asymptotic range would not be observed. An example of this occurred in a coupled thermal-mechanical problem in which the initial attempts to assess convergence had too high of a thermal load [Cox and Mish 2013].

As discussed in Section 3.3, with the increased loading and the corresponding increased importance of the nonlinearities, the manufactured solution increases the magnitude of the body loads to constrain the displacement response to match that of the linear elastic solution. This trend is depicted in Figures Figure 21 and Figure 22 which depict the distributions of body loads, at the two bounds of the load level (3 ksi and 60 ksi).

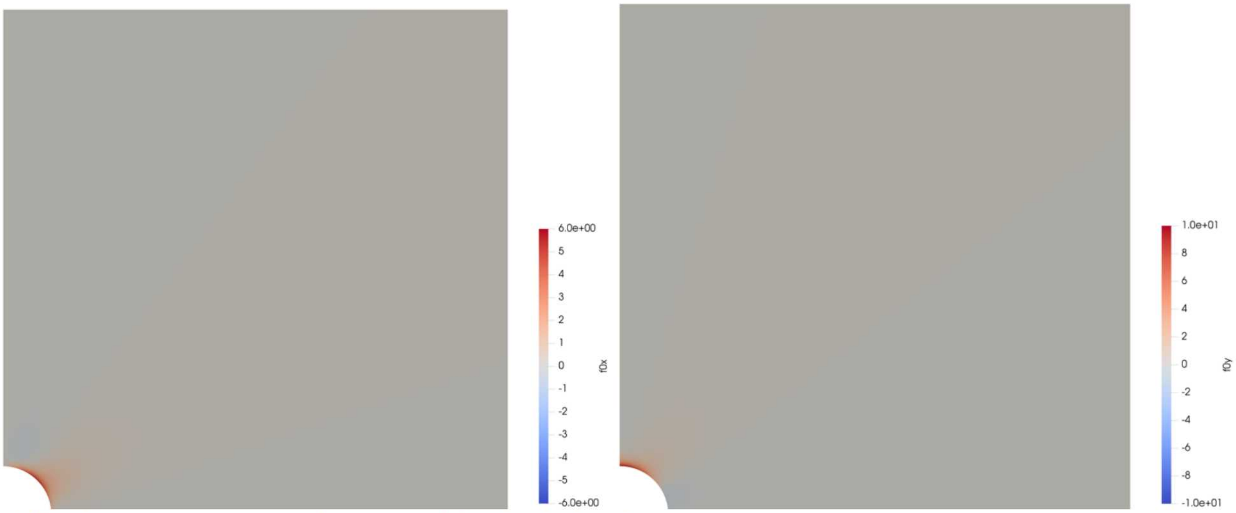

*(a) Scales to capture maximum positive body loads.*

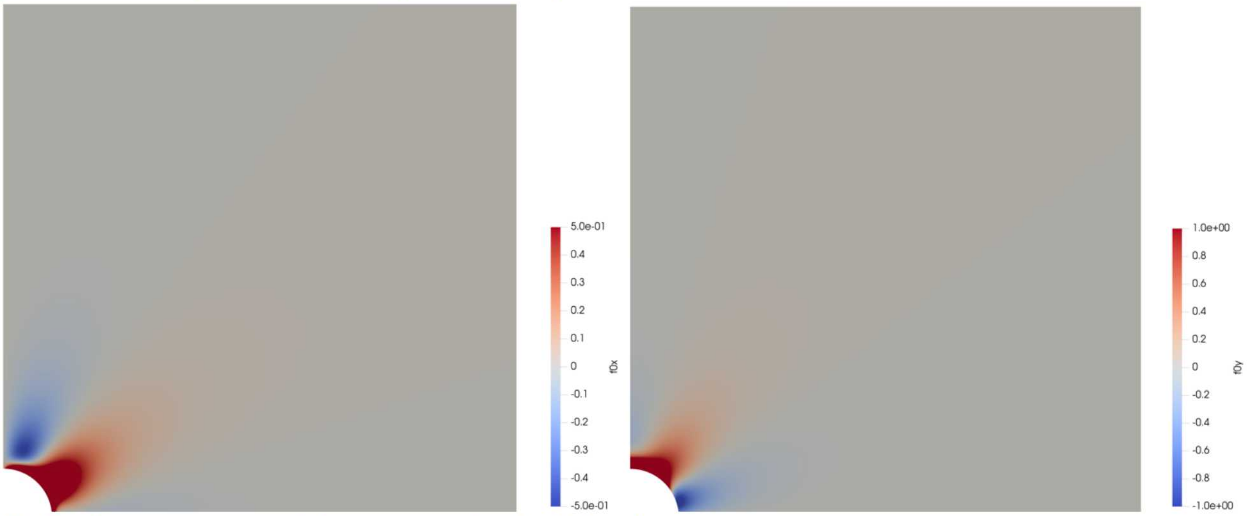

*(b) Scales to capture minimum negative body loads.*

*Figure 21. Body load components for T=3 ksi load level – multiple scales (x component on left, y on right).*

In each set of figures, two scales are used to highlight the maximum positive body load component in each coordinate direction and the minimum negative body loads. Comparing the results at the two load levels, note that the magnitudes of the body force loads are quite different but the distributions appear to be almost identical (to the naked eye). Examining the magnitudes from both figures indicates that the size of the body loads is very nonlinear with respect to the loading level.

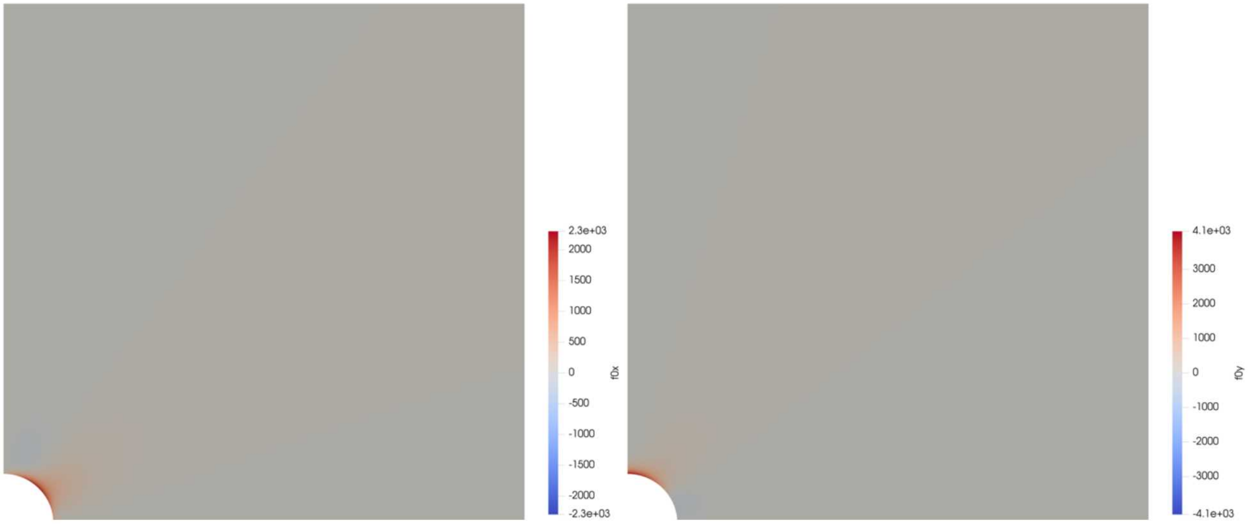

*(a) Scales to capture maximum positive body loads.*

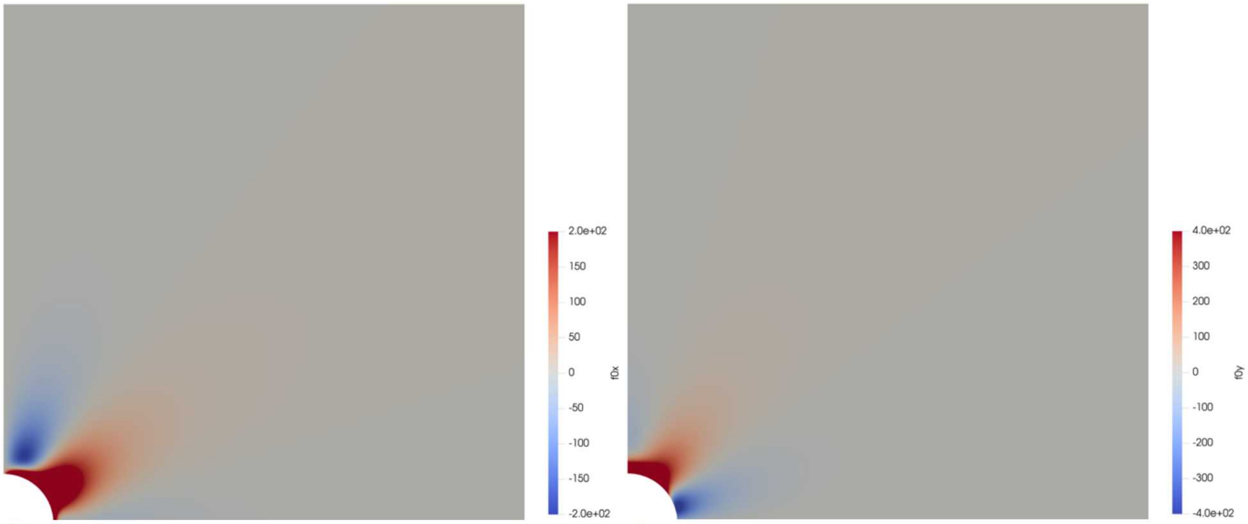

*(b) Scales to capture minimum negative body loads.*

*Figure 22. Body load components for T=60 ksi load level – multiple scales (x component on left, y on right)*

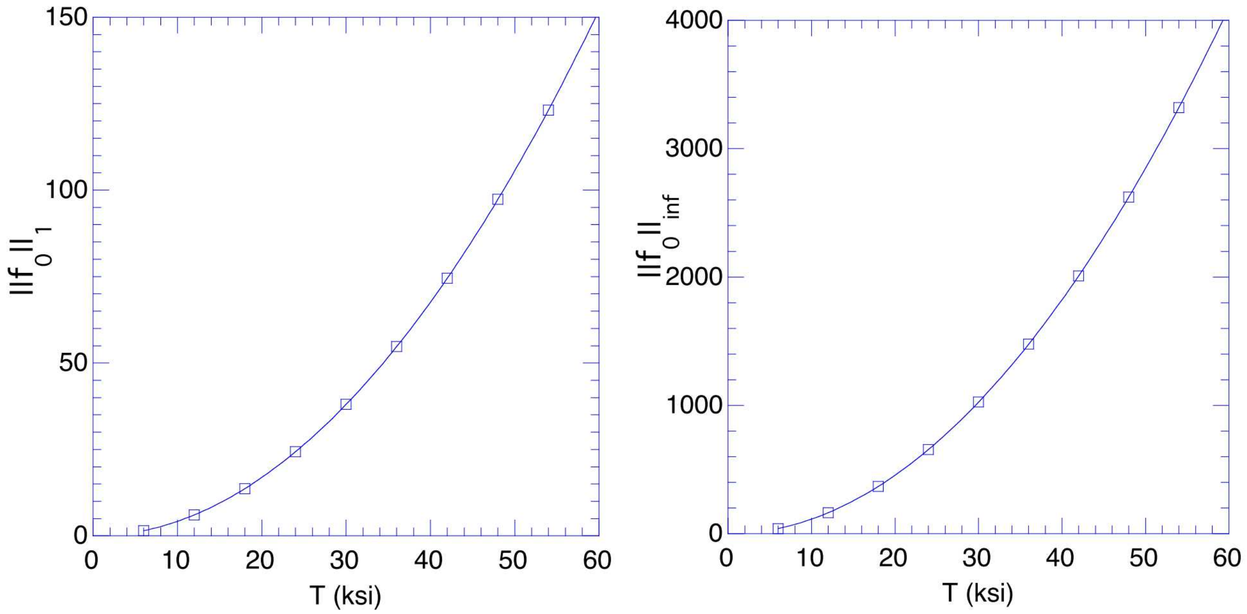

*Figure 23. Norms of the body loads for the manufactured solution as a function of the traction level.*

To more clearly illustrate the nonlinearity of the body load, Figure 23 shows two norms of the body loads as functions of the traction level. Note that the $||.||_\infty$ measures the maximum body loads for a given distribution while $||.||_1$ "more directly" measures the size of the whole field. The results clearly reflect the nonlinearity that has its origins in the nonlinearity of the governing equations. The expressions in Appendix I, show the body loads are at least quadratic in ***T***. The trend also reflects the fact that as the traction load approaches zero, the body loads approach zero, thus rendering the original classical problem as the contributions in the nonlinearities of the governing equations become insignificant relative to the linear terms.

# 5. CLOSING SUMMARY

Previous verification results for Sierra/SM using inexact reference solutions often exhibited unsatisfactory convergence behavior. Without a more complete understanding of the convergence behavior of these types of tests, one can falsely attribute pathologies of the test with incorrectness of the code. These tests provide a weaker measure of the code correctness, since the source of the observed convergence issues is uncertain. Fortunately, understanding the effects of using an inexact reference solution can allow one to better interpret the convergence behavior, thus increasing the credibility of the code.

Inexactness of the reference solution can result from the solution solving a different set of governing equations (*e.g.*, linear elasticity *vs*. the fully nonlinear equations), approximations made in the solving the mathematical equations (*e.g.*, approximations in Hertz contact theory), or approximations made in the computational model (*e.g.*, finite *vs*. infinite domain).

Convergence results measured with an inexact reference solution can have three regions in a convergence plot: *pre-asymptotic range*, *apparent asymptotic range*, and the *inaccurate reference range*. Simple theoretical results examining the norms of errors highlight that for an inexact reference solution two conditions must be met to observe asymptotic convergence: (1) the solutions must be in the asymptotic range (with respect to the exact solution), and (2) the reference solution must be sufficiently close to the exact solution. The *pre-asymptotic range* results when higher order error terms are not sufficiently small for relatively coarse meshes; in contrast, the *inaccurate reference range* will occur for relatively fine meshes. In this later case when the mesh is sufficiently fine, the true error (referencing the exact solution) differs too much from the apparent error (referencing the inexact reference solution) for the inexact reference solution to be an accurate surrogate, and the apparent error converges to a fixed value. When the code does not have an error, this fixed value is the error in the reference solution relative to the exact solution. As such, an inherent difficultly when using an inexact reference solution is finding a “sweet spot” in the range of the mesh densities that are not too coarse and not too fine to exhibit the asymptotic behavior. A lack of apparent convergence does not necessarily imply a code error exists. This uncertainty in how to interpret some convergence results is why these are weaker convergence tests compared to tests with exact solutions.

Simple graphical examples of convergence were used to explain the variation in convergence behaviors that one can observe when using an inexact reference solution, ranging from having the three distinct ranges with monotonic convergence to results that appear to be divergent over the full range of meshes. The nature of the convergence behavior depends upon the relative accuracy of the reference solution, the relative orientations of the reference and the exact solutions (as vectors in a function space), the theoretical rate of convergence of the response, and the selected sequence of meshes.

The hole in the plate problem is an actual example of how problematic this type of verification problem can be. Initial results did not indicate the code was converging. Manufacturing a solution for the problem showed the code was convergent. A study of the boundary conditions showed the initial approximation for the finite domain while sufficiently accurate for engineering results, yielded an exact solution that deviated too much from the reference solution to be able to measure convergence. Refinements to the boundary conditions to match those of the manufactured solution yielded significant ranges over which the asymptotic range of the solutions could be measured. Nonetheless, if the mesh was refined enough or the load was increased enough the importance of the nonlinearities in the solution would result in an apparent divergence behavior with the error converging to a constant value (characteristic of the inaccurate reference range). The problem also demonstrated the nonlinearity of the manufactured body loads as a function of the load level, a direct result of the nonlinearity in the governing equations.

The verification analyst can either try to adjust the computational models (*e.g.*, domain size, boundary conditions, or meshes) to attain an apparent asymptotic range of convergence or manufacture a solution to eliminate the inaccuracies that will pollute the convergence results with sufficient mesh refinement. The relative efficiency of each approach is highly problem dependent. The former approach generally has a simpler reference solution, but the later approach gives a stronger verification test, often to a more general problem (*e.g.*, including finite deformations).

# 6. REFERENCES

Bonet J, Wood RD. *Nonlinear Continuum Mechanics for Finite Element Analysis* ($2^{nd}$ ed.). Cambridge University Press: Cambridge UK, 2008.

Copps KD, Carnes BR. Sierra Verification Module: Encore User Guide – Version 4.34, *2014-XXXX*, Sandia National Laboratories, Albuquerque, NM, 2014; 246.

Cox JV. Manufactured Solutions for Solid Mechanics Code Verification – Hyperelastic Material Case. *SAND Report 2016-9591*, Sandia National Laboratories, Albuquerque, NM, 2016; 36.

Cox JV, Mish KD. Sierra Solid Mechanics Example Verification Problems to Highlight the use of Sierra Verification Tools. *SAND Report 2013-2390*, Sandia National Laboratories, Albuquerque, NM, 2013; 122.

Muskhelishvili NI. *Some Basic Problems of the Mathematical Theory of Elasticity*. P. Noordhoff Ltd., Groningen, Holland, 1953; 704.

Oden JT. *Applied Functional Analysis – A First Course for Students in Mechanics and Engineering Science*, Prentice-Hall, Inc., Englewood Cliffs, New Jersey, 1979.

Orient GE, Alvis T. Unpublished presentation on Sierra/SM Code Verification based upon the Classical Elasticity Solution of a Hole in a Plate, August 2017.

Sierra/SM Team, Sierra/SolidMechanics 4.48, Verification Tests Manual. SAND Report 2018-2341, Sandia National Laboratories, Albuquerque, NM, March 2018; 448.

Sokolnikoff IS. *Mathematical Theory of Elasticity*. Robert E. Krieger Publishing Company, Malabar Florida, 1956; 476. Stakgold I. *Green's Functions and Boundary Value Problems*, John Wiley & Sons, New York, 1979.

# APPENDIX I: EXAMPLE OUTPUT FROM THE HYPERELASTIC FACTORY

This appendix contains a few of the expressions output from the hyperelastic factory that became too complicated to merit type-setting, namely the Cauchy stresses and material body loads.

The nomenclature for the following equations is consistent with the main text, and the additional elastic constant $\lambda$ is the first Lame constant from the generalized Hooke's law for an isotropic body (*ref. e.g.*, Sokolnikoff [1956]).

# Cauchy Stress Components

$\sigma_{11}$

$$\Bigg(\left(X_1^2+X_2^2\right)^4 \Bigg(\Bigg(T+T\kappa+8\mu+\frac{1}{\left(X_1^2+X_2^2\right)^4}2a^2T\left(3a^2X_1^4-(2+\kappa)X_1^6-X_1^2\left(18a^2+(-10+\kappa)X_1^2\right)X_2^2+\left(3a^2+(10+\kappa)X_1^2\right)X_2^4+(-2+\kappa)X_2^6\right)\Bigg)$$

$$\Bigg(1/\left(X_1^2+X_2^2\right)^{10}a^4T^2X_1^2X_2^2\left(6a^2X_1^2-(6+\kappa)X_1^4-2\left(3a^2+(2+\kappa)X_1^2\right)X_2^2-(-2+\kappa)X_2^4\right)$$

$$((T(3-7\kappa)-40\mu)X_1^8+6a^4T(1-3\kappa)X_2^4+2a^2(T+T\kappa-24\mu)X_2^6+(T(-5+\kappa)+24\mu)X_2^8+$$

$$2X_1^6\left(a^2(T(-5+11\kappa)+24\mu)+2(T-5T\kappa-24\mu)X_2^2\right)+2X_1^2X_2^2\Big(6a^4T(1+5\kappa)-a^2(T(3+19\kappa)+24\mu)$$

$$X_2^2-2(T(3+\kappa)-8\mu)X_2^4\Big)+6X_1^4\left(a^4T(1-3\kappa)+a^2(-3T(1+\kappa)+8\mu)X_2^2-(T+3T\kappa+8\mu)X_2^4\right))+2\mu$$

$$\Bigg(T+T\kappa+8\mu+\frac{1}{\left(X_1^2+X_2^2\right)^4}2a^2T\left(3a^2X_1^4-(2+\kappa)X_1^6-X_1^2\left(18a^2+(-10+\kappa)X_1^2\right)X_2^2+\left(3a^2+(10+\kappa)X_1^2\right)X_2^4+(-2+\kappa)X_2^6\right)\Bigg)$$

$$\Bigg(1/\left(64\mu^2\right)T\lambda\Bigg(5T-2T\kappa+T\kappa^2-16\mu+16\kappa\mu+\frac{4a^4T\left(9a^4-12a^2X_1^2-16(-3+\kappa)X_1^4\right)}{\left(X_1^2+X_2^2\right)^4}-$$

$$\frac{8a^2T\left(3a^4+4a^2(5-2\kappa)X_1^2+16X_1^4\right)}{\left(X_1^2+X_2^2\right)^3}+\frac{1}{\left(X_1^2+X_2^2\right)^2}(4a^4T(8+(-2+\kappa)\kappa)-$$

$$8a^2(T(-13+(-2+\kappa)\kappa)+8(-1+\kappa)\mu)X_1^2)+\frac{4a^2(T(-1+(-2+\kappa)\kappa)+8(-1+\kappa)\mu)}{X_1^2+X_2^2}\Bigg)+\mu\Bigg(-1+1/\left(64\mu^2\right)$$

$$\Bigg(\frac{1}{\left(X_1^2+X_2^2\right)^8}16a^4T^2X_1^2X_2^2\left((-4+\kappa)X_1^4-6a^2X_2^2+(4+\kappa)X_2^4+2X_1^2\left(3a^2+\kappa X_2^2\right)\right)^2+\Bigg(T+T\kappa+8\mu+\frac{1}{\left(X_1^2+X_2^2\right)^4}$$

$$2a^2T\left(3a^2X_1^4-(2+\kappa)X_1^6-X_1^2\left(18a^2+(-10+\kappa)X_1^2\right)X_2^2+\left(3a^2+(10+\kappa)X_1^2\right)X_2^4+(-2+\kappa)X_2^6\right)\Bigg)^2\Bigg)\Bigg)\Bigg)\Bigg)\Bigg)+$$

$$1/\left(X_1^2+X_2^2\right)^{10}a^4T^2X_1^2X_2^2\left(6a^2X_1^2-(6+\kappa)X_1^4-2\left(3a^2+(2+\kappa)X_1^2\right)X_2^2-(-2+\kappa)X_2^4\right)$$

$$\Bigg(((T(3-7\kappa)-40\mu)X_1^8+6a^4T(1-3\kappa)X_2^4+2a^2(T+T\kappa-24\mu)X_2^6+$$

$$(T(-5+\kappa)+24\mu)X_2^8+2X_1^6\left(a^2(T(-5+11\kappa)+24\mu)+2(T-5T\kappa-24\mu)X_2^2\right)+$$

$$2X_1^2X_2^2\left(6a^4T(1+5\kappa)-a^2(T(3+19\kappa)+24\mu)X_2^2-2(T(3+\kappa)-8\mu)X_2^4\right)+$$

$$6X_1^4\left(a^4T(1-3\kappa)+a^2(-3T(1+\kappa)+8\mu)X_2^2-(T+3T\kappa+8\mu)X_2^4\right))\Bigg(T+T\kappa+8\mu+\frac{1}{\left(X_1^2+X_2^2\right)^4}$$

$$2a^2T\left(3a^2X_1^4-(2+\kappa)X_1^6-X_1^2\left(18a^2+(-10+\kappa)X_1^2\right)X_2^2+\left(3a^2+(10+\kappa)X_1^2\right)X_2^4+(-2+\kappa)X_2^6\right)\Bigg)+$$

$$32\mu\left(X_1^2+X_2^2\right)^2\left(6a^2X_1^2-(6+\kappa)X_1^4-2\left(3a^2+(2+\kappa)X_1^2\right)X_2^2-(-2+\kappa)X_2^4\right)$$

$$\Bigg(1/\left(64\mu^2\right)T\lambda\Bigg(5T-2T\kappa+T\kappa^2-16\mu+16\kappa\mu+\frac{4a^4T\left(9a^4-12a^2X_1^2-16(-3+\kappa)X_1^4\right)}{\left(X_1^2+X_2^2\right)^4}-$$

$$\frac{8a^2T\left(3a^4+4a^2(5-2\kappa)X_1^2+16X_1^4\right)}{\left(X_1^2+X_2^2\right)^3}+\frac{1}{\left(X_1^2+X_2^2\right)^2}(4a^4T(8+(-2+\kappa)\kappa)-8a^2(T(-13+(-2+\kappa)\kappa)+$$

$$8(-1+\kappa)\mu)X_1^2)+\frac{4a^2(T(-1+(-2+\kappa)\kappa)+8(-1+\kappa)\mu)}{X_1^2+X_2^2}\Bigg)+\mu\Bigg(-1+1/\left(64\mu^2\right)\Bigg(\frac{1}{\left(X_1^2+X_2^2\right)^8}$$

$$16a^4T^2X_1^2X_2^2\left((6+\kappa)X_1^4+6a^2X_2^2+(-2+\kappa)X_2^4+X_1^2\left(-6a^2+2(2+\kappa)X_2^2\right)\right)^2+\Bigg(T(-3+\kappa)+8\mu-\frac{1}{\left(X_1^2+X_2^2\right)^4}$$

$$2a^2T\left((-4+\kappa)X_1^6+3a^2X_2^4-\kappa X_2^6+X_1^4\left(3a^2+(8+\kappa)X_2^2\right)-X_1^2\left(18a^2X_2^2+(-12+\kappa)X_2^4\right)\right)\Bigg)^2\Bigg)\Bigg)\Bigg)\Bigg)\Bigg)\Bigg)\Bigg)\Big/$$

$$\Big(2\mu\Big((T(-3+\kappa)+8\mu)(T+T\kappa+8\mu)X_1^8+4X_1^6\Big(a^2T(T(5-(-2+\kappa)\kappa)-8(-1+\kappa)\mu)+$$

$$(T(-3+\kappa)+8\mu)(T+T\kappa+8\mu)X_2^2\Big)-$$

$$\left(6a^4T-2a^2T\kappa X_2^2-(T(-3+\kappa)+8\mu)X_2^4\right)\left(6a^4T+2a^2T(-2+\kappa)X_2^2+(T+T\kappa+8\mu)X_2^4\right)+$$

$$2$$

$$X_1^4$$

$$\Big(2a^4T^2(-14+(-2+\kappa)\kappa)-2a^2T(T(19+(-2+\kappa)\kappa)+8(-1+\kappa)\mu)X_2^2+$$

$$3(T(-3+\kappa)+8\mu)(T+T\kappa+8\mu)X_2^4\Big)+$$

$$4X_1^2\Big(18a^6T^2+2a^4T^2(14+\kappa(6+\kappa))X_2^2+a^2T(T(-21+(-2+\kappa)\kappa)+8(-1+\kappa)\mu)X_2^4+$$

$$(T(-3+\kappa)+8\mu)(T+T\kappa+8\mu)X_2^6\Big)\Big)\Big)$$

$\underline{\sigma_{12}}$

$$(a^2 T X_1 X_2 (16 (X_1^2+X_2^2)^2 ((-4+\kappa) X_1^4 - 6 a^2 X_2^2 + (4+\kappa) X_2^4 + 2 X_1^2 (3 a^2 + \kappa X_2^2))$$

$$(1/(X_1^2+X_2^2)^{10} a^4 T^2 X_1^2 X_2^2 (6 a^2 X_1^2 - (6+\kappa) X_1^4 - 2 (3 a^2 + (2+\kappa) X_1^2) X_2^2 - (-2+\kappa) X_2^4)$$

$$((T (3-7\kappa) - 40\mu) X_1^8 + 6 a^4 T (1-3\kappa) X_2^4 + 2 a^2 (T + T\kappa - 24\mu) X_2^6 + (T (-5+\kappa) + 24\mu) X_2^8 +$$

$$2 X_1^6 (a^2 (T (-5+11\kappa) + 24\mu) + 2 (T - 5 T\kappa - 24\mu) X_2^2) + 2 X_1^2 X_2^2 (6 a^4 T (1+5\kappa) - a^2 (T (3+19\kappa) + 24\mu)$$

$$X_2^2 - 2 (T (3+\kappa) - 8\mu) X_2^4) + 6 X_1^4 (a^4 T (1-3\kappa) + a^2 (-3 T (1+\kappa) + 8\mu) X_2^2 - (T + 3 T\kappa + 8\mu) X_2^4)) + 2\mu$$

$$(T + T\kappa + 8\mu + \frac{1}{(X_1^2+X_2^2)^4} 2 a^2 T (3 a^2 X_1^4 - (2+\kappa) X_1^6 - X_1^2 (18 a^2 + (-10+\kappa) X_1^2) X_2^2 + (3 a^2 + (10+\kappa) X_1^2) X_2^4 + (-2+\kappa) X_2^6))$$

$$(1/(64\mu^2) T\lambda (5 T - 2 T\kappa + T\kappa^2 - 16\mu + 16\kappa\mu + \frac{4 a^4 T (9 a^4 - 12 a^2 X_1^2 - 16 (-3+\kappa) X_1^4)}{(X_1^2+X_2^2)^4} -$$

$$\frac{8 a^2 T (3 a^4 + 4 a^2 (5-2\kappa) X_1^2 + 16 X_1^4)}{(X_1^2+X_2^2)^3} + \frac{1}{(X_1^2+X_2^2)^2} (4 a^4 T (8 + (-2+\kappa)\kappa) -$$

$$8 a^2 (T (-13 + (-2+\kappa)\kappa) + 8 (-1+\kappa)\mu) X_1^2) + \frac{4 a^2 (T (-1 + (-2+\kappa)\kappa) + 8 (-1+\kappa)\mu)}{X_1^2+X_2^2}) + \mu (-1 + 1/(64\mu^2)$$

$$(\frac{1}{(X_1^2+X_2^2)^8} 16 a^4 T^2 X_1^2 X_2^2 ((-4+\kappa) X_1^4 - 6 a^2 X_2^2 + (4+\kappa) X_2^4 + 2 X_1^2 (3 a^2 + \kappa X_2^2))^2 + (T + T\kappa + 8\mu + \frac{1}{(X_1^2+X_2^2)^4}$$

$$2 a^2 T (3 a^2 X_1^4 - (2+\kappa) X_1^6 - X_1^2 (18 a^2 + (-10+\kappa) X_1^2) X_2^2 + (3 a^2 + (10+\kappa) X_1^2) X_2^4 + (-2+\kappa) X_2^6))^2)))) +$$

$$(T (-3+\kappa) + 8\mu - \frac{1}{(X_1^2+X_2^2)^4} 2 a^2 T ((-4+\kappa) X_1^6 + 3 a^2 X_2^4 - \kappa X_2^6 + X_1^4 (3 a^2 + (8+\kappa) X_2^2) - X_1^2 (18 a^2 X_2^2 + (-12+\kappa) X_2^4)))$$

$$(((T (3-7\kappa) - 40\mu) X_1^8 + 6 a^4 T (1-3\kappa) X_2^4 + 2 a^2 (T + T\kappa - 24\mu) X_2^6 +$$

$$(T (-5+\kappa) + 24\mu) X_2^8 + 2 X_1^6 (a^2 (T (-5+11\kappa) + 24\mu) + 2 (T - 5 T\kappa - 24\mu) X_2^2) +$$

$$2 X_1^2 X_2^2 (6 a^4 T (1+5\kappa) - a^2 (T (3+19\kappa) + 24\mu) X_2^2 - 2 (T (3+\kappa) - 8\mu) X_2^4) +$$

$$6 X_1^4 (a^4 T (1-3\kappa) + a^2 (-3 T (1+\kappa) + 8\mu) X_2^2 - (T + 3 T\kappa + 8\mu) X_2^4)) (T + T\kappa + 8\mu + \frac{1}{(X_1^2+X_2^2)^4}$$

$$2 a^2 T (3 a^2 X_1^4 - (2+\kappa) X_1^6 - X_1^2 (18 a^2 + (-10+\kappa) X_1^2) X_2^2 + (3 a^2 + (10+\kappa) X_1^2) X_2^4 + (-2+\kappa) X_2^6)) +$$

$$32\mu (X_1^2+X_2^2)^2 (6 a^2 X_1^2 - (6+\kappa) X_1^4 - 2 (3 a^2 + (2+\kappa) X_1^2) X_2^2 - (-2+\kappa) X_2^4)$$

$$(1/(64\mu^2) T\lambda (5 T - 2 T\kappa + T\kappa^2 - 16\mu + 16\kappa\mu + \frac{4 a^4 T (9 a^4 - 12 a^2 X_1^2 - 16 (-3+\kappa) X_1^4)}{(X_1^2+X_2^2)^4} -$$

$$\frac{8 a^2 T (3 a^4 + 4 a^2 (5-2\kappa) X_1^2 + 16 X_1^4)}{(X_1^2+X_2^2)^3} + \frac{1}{(X_1^2+X_2^2)^2} (4 a^4 T (8 + (-2+\kappa)\kappa) - 8 a^2 (T (-13 + (-2+\kappa)\kappa) +$$

$$8 (-1+\kappa)\mu) X_1^2) + \frac{4 a^2 (T (-1 + (-2+\kappa)\kappa) + 8 (-1+\kappa)\mu)}{X_1^2+X_2^2}) + \mu (-1 + 1/(64\mu^2) (\frac{1}{(X_1^2+X_2^2)^8}$$

$$16 a^4 T^2 X_1^2 X_2^2 ((6+\kappa) X_1^4 + 6 a^2 X_2^2 + (-2+\kappa) X_2^4 + X_1^2 (-6 a^2 + 2 (2+\kappa) X_2^2))^2 + (T (-3+\kappa) + 8\mu - \frac{1}{(X_1^2+X_2^2)^4}$$

$$2 a^2 T ((-4+\kappa) X_1^6 + 3 a^2 X_2^4 - \kappa X_2^6 + X_1^4 (3 a^2 + (8+\kappa) X_2^2) - X_1^2 (18 a^2 X_2^2 + (-12+\kappa) X_2^4)))^2)))))) /$$

$$(8\mu (X_1^2+X_2^2)^2 ((T (-3+\kappa) + 8\mu) (T + T\kappa + 8\mu) X_1^8 + 4 X_1^6 (a^2 T (T (5 - (-2+\kappa)\kappa) - 8 (-1+\kappa)\mu) +$$

$$(T (-3+\kappa) + 8\mu) (T + T\kappa + 8\mu) X_2^2) -$$

$$(6 a^4 T - 2 a^2 T\kappa X_2^2 - (T (-3+\kappa) + 8\mu) X_2^4) (6 a^4 T + 2 a^2 T (-2+\kappa) X_2^2 + (T + T\kappa + 8\mu) X_2^4) +$$

$$2$$

$$X_1^4$$

$$(2 a^4 T^2 (-14 + (-2+\kappa)\kappa) - 2 a^2 T (T (19 + (-2+\kappa)\kappa) + 8 (-1+\kappa)\mu) X_2^2 +$$

$$3 (T (-3+\kappa) + 8\mu) (T + T\kappa + 8\mu) X_2^4) +$$

$$4 X_1^2 (18 a^6 T^2 + 2 a^4 T^2 (14 + \kappa (6+\kappa)) X_2^2 + a^2 T (T (-21 + (-2+\kappa)\kappa) + 8 (-1+\kappa)\mu) X_2^4 +$$

$$(T (-3+\kappa) + 8\mu) (T + T\kappa + 8\mu) X_2^6)))$$

$\underline{\sigma_{22}}$

$$\Big(\left(X_1^2+X_2^2\right)^4$$

$$\Big(1/\left(X_1^2+X_2^2\right)^{10} a^4 T^2 X_1^2 X_2^2 \left((-4+\kappa) X_1^4-6 a^2 X_2^2+(4+\kappa) X_2^4+2 X_1^2 \left(3 a^2+\kappa X_2^2\right)\right) \Big(\big((T (3-7 \kappa)-40 \mu) X_1^8+6 a^4 T (1-3 \kappa) X_2^4+$$

$$2 a^2 (T+T \kappa-24 \mu) X_2^6+(T (-5+\kappa)+24 \mu) X_2^8+2 X_1^6 \left(a^2 (T (-5+11 \kappa)+24 \mu)+2 (T-5 T \kappa-24 \mu) X_2^2\right)+$$

$$2 X_1^2 X_2^2 \left(6 a^4 T (1+5 \kappa)-a^2 (T (3+19 \kappa)+24 \mu) X_2^2-2 (T (3+\kappa)-8 \mu) X_2^4\right)+$$

$$6 X_1^4 \left(a^4 T (1-3 \kappa)+a^2 (-3 T (1+\kappa)+8 \mu) X_2^2-(T+3 T \kappa+8 \mu) X_2^4\right)\big)$$

$$\left(T (-3+\kappa)+8 \mu-\frac{1}{\left(X_1^2+X_2^2\right)^4} 2 a^2 T \left((-4+\kappa) X_1^6+3 a^2 X_2^4-\kappa X_2^6+X_1^4 \left(3 a^2+(8+\kappa) X_2^2\right)-X_1^2 \left(18 a^2 X_2^2+(-12+\kappa) X_2^4\right)\right)\right)+$$

$$32 \mu \left(X_1^2+X_2^2\right)^2 \left((-4+\kappa) X_1^4-6 a^2 X_2^2+(4+\kappa) X_2^4+2 X_1^2 \left(3 a^2+\kappa X_2^2\right)\right)$$

$$\Big(1/\left(64 \mu^2\right) T \lambda \Big(5 T-2 T \kappa+T \kappa^2-16 \mu+16 \kappa \mu+\frac{4 a^4 T \left(9 a^4-12 a^2 X_1^2-16 (-3+\kappa) X_1^4\right)}{\left(X_1^2+X_2^2\right)^4}-$$

$$\frac{8 a^2 T \left(3 a^4+4 a^2 (5-2 \kappa) X_1^2+16 X_1^4\right)}{\left(X_1^2+X_2^2\right)^3}+\frac{1}{\left(X_1^2+X_2^2\right)^2}\big(4 a^4 T (8+(-2+\kappa) \kappa)-8 a^2$$

$$(T (-13+(-2+\kappa) \kappa)+8 (-1+\kappa) \mu) X_1^2\big)+\frac{4 a^2 (T (-1+(-2+\kappa) \kappa)+8 (-1+\kappa) \mu)}{X_1^2+X_2^2}\Big)+\mu \Big(-1+1/\left(64 \mu^2\right)$$

$$\Big(\frac{1}{\left(X_1^2+X_2^2\right)^8} 16 a^4 T^2 X_1^2 X_2^2 \left((-4+\kappa) X_1^4-6 a^2 X_2^2+(4+\kappa) X_2^4+2 X_1^2 \left(3 a^2+\kappa X_2^2\right)\right)^2+\Big(T+T \kappa+8 \mu+\frac{1}{\left(X_1^2+X_2^2\right)^4}$$

$$2 a^2 T \left(3 a^2 X_1^4-(2+\kappa) X_1^6-X_1^2 \left(18 a^2+(-10+\kappa) X_1^2\right) X_2^2+\left(3 a^2+(10+\kappa) X_1^2\right) X_2^4+(-2+\kappa) X_2^6\right)\Big)^2\Big)\Big)\Big)\Big)+$$

$$\left(T (-3+\kappa)+8 \mu-\frac{1}{\left(X_1^2+X_2^2\right)^4} 2 a^2 T \left((-4+\kappa) X_1^6+3 a^2 X_2^4-\kappa X_2^6+X_1^4 \left(3 a^2+(8+\kappa) X_2^2\right)-X_1^2 \left(18 a^2 X_2^2+(-12+\kappa) X_2^4\right)\right)\right)$$

$$\Big(1/\left(X_1^2+X_2^2\right)^{10} a^4 T^2 X_1^2 X_2^2 \left((-4+\kappa) X_1^4-6 a^2 X_2^2+(4+\kappa) X_2^4+2 X_1^2 \left(3 a^2+\kappa X_2^2\right)\right) \big((T (3-7 \kappa)-40 \mu) X_1^8+6 a^4 T (1-3 \kappa) X_2^4+$$

$$2 a^2 (T+T \kappa-24 \mu) X_2^6+(T (-5+\kappa)+24 \mu) X_2^8+2 X_1^6 \left(a^2 (T (-5+11 \kappa)+24 \mu)+2 (T-5 T \kappa-24 \mu) X_2^2\right)+$$

$$2 X_1^2 X_2^2 \left(6 a^4 T (1+5 \kappa)-a^2 (T (3+19 \kappa)+24 \mu) X_2^2-2 (T (3+\kappa)-8 \mu) X_2^4\right)+$$

$$6 X_1^4 \left(a^4 T (1-3 \kappa)+a^2 (-3 T (1+\kappa)+8 \mu) X_2^2-(T+3 T \kappa+8 \mu) X_2^4\right)\big)+$$

$$2 \mu \left(T (-3+\kappa)+8 \mu-\frac{1}{\left(X_1^2+X_2^2\right)^4} 2 a^2 T \left((-4+\kappa) X_1^6+3 a^2 X_2^4-\kappa X_2^6+X_1^4 \left(3 a^2+(8+\kappa) X_2^2\right)-X_1^2 \left(18 a^2 X_2^2+(-12+\kappa) X_2^4\right)\right)\right)$$

$$\Big(1/\left(64 \mu^2\right) T \lambda \Big(5 T-2 T \kappa+T \kappa^2-16 \mu+16 \kappa \mu+\frac{4 a^4 T \left(9 a^4-12 a^2 X_1^2-16 (-3+\kappa) X_1^4\right)}{\left(X_1^2+X_2^2\right)^4}-$$

$$\frac{8 a^2 T \left(3 a^4+4 a^2 (5-2 \kappa) X_1^2+16 X_1^4\right)}{\left(X_1^2+X_2^2\right)^3}+\frac{1}{\left(X_1^2+X_2^2\right)^2}\big(4 a^4 T (8+(-2+\kappa) \kappa)-8 a^2 (T (-13+(-2+\kappa) \kappa)+$$

$$8 (-1+\kappa) \mu) X_1^2\big)+\frac{4 a^2 (T (-1+(-2+\kappa) \kappa)+8 (-1+\kappa) \mu)}{X_1^2+X_2^2}\Big)+\mu \Big(-1+1/\left(64 \mu^2\right) \Big(\frac{1}{\left(X_1^2+X_2^2\right)^8}$$

$$16 a^4 T^2 X_1^2 X_2^2 \left((6+\kappa) X_1^4+6 a^2 X_2^2+(-2+\kappa) X_2^4+X_1^2 \left(-6 a^2+2 (2+\kappa) X_2^2\right)\right)^2+\Big(T (-3+\kappa)+8 \mu-\frac{1}{\left(X_1^2+X_2^2\right)^4}$$

$$2 a^2 T \left((-4+\kappa) X_1^6+3 a^2 X_2^4-\kappa X_2^6+X_1^4 \left(3 a^2+(8+\kappa) X_2^2\right)-X_1^2 \left(18 a^2 X_2^2+(-12+\kappa) X_2^4\right)\right)\Big)^2\Big)\Big)\Big)\Big)\Big)\Big)/$$

$$\Big(2 \mu \Big((T (-3+\kappa)+8 \mu) (T+T \kappa+8 \mu) X_1^8+4 X_1^6 \left(a^2 T (T (5-(-2+\kappa) \kappa)-8 (-1+\kappa) \mu)+(T (-3+\kappa)+8 \mu) (T+T \kappa+8 \mu) X_2^2\right)-$$

$$\left(6 a^4 T-2 a^2 T \kappa X_2^2-(T (-3+\kappa)+8 \mu) X_2^4\right)$$

$$\left(6 a^4 T+2 a^2 T (-2+\kappa) X_2^2+(T+T \kappa+8 \mu) X_2^4\right)+$$

$$2 X_1^4 \big(2 a^4 T^2 (-14+(-2+\kappa) \kappa)-2 a^2 T (T (19+(-2+\kappa) \kappa)+8 (-1+\kappa) \mu) X_2^2+$$

$$3 (T (-3+\kappa)+8 \mu) (T+T \kappa+8 \mu) X_2^4\big)+$$

$$4 X_1^2 \big(18 a^6 T^2+2 a^4 T^2 (14+\kappa (6+\kappa)) X_2^2+a^2 T (T (-21+(-2+\kappa) \kappa)+8 (-1+\kappa) \mu) X_2^4+$$

$$(T (-3+\kappa)+8 \mu) (T+T \kappa+8 \mu) X_2^6\big)\Big)\Big)$$

σ33

$$
\begin{aligned}
&\left(T\lambda\left(X_1^2+X_2^2\right)^4\left(5T-2T\kappa+T\kappa^2-16\mu+16\kappa\mu+\frac{4a^4T\left(9a^4-12a^2X_1^2-16(-3+\kappa)X_1^4\right)}{\left(X_1^2+X_2^2\right)^4}-\frac{8a^2T\left(3a^4+4a^2(5-2\kappa)X_1^2+16X_1^4\right)}{\left(X_1^2+X_2^2\right)^3}+\right.\right.\\
&\qquad\left.\left.\frac{4a^4T(8+(-2+\kappa)\kappa)-8a^2(T(-13+(-2+\kappa)\kappa)+8(-1+\kappa)\mu)X_1^2}{\left(X_1^2+X_2^2\right)^2}+\frac{4a^2(T(-1+(-2+\kappa)\kappa)+8(-1+\kappa)\mu)}{X_1^2+X_2^2}\right)\right)\Big/\\
&\Big((T(-3+\kappa)+8\mu)(T+T\kappa+8\mu)X_1^8+4X_1^6\left(a^2T(T(5-(-2+\kappa)\kappa)-8(-1+\kappa)\mu)+(T(-3+\kappa)+8\mu)(T+T\kappa+8\mu)X_2^2\right)-\\
&\quad\left(6a^4T-2a^2T\kappa X_2^2-(T(-3+\kappa)+8\mu)X_2^4\right)\left(6a^4T+2a^2T(-2+\kappa)X_2^2+(T+T\kappa+8\mu)X_2^4\right)+\\
&\quad 2X_1^4\left(2a^4T^2(-14+(-2+\kappa)\kappa)-2a^2T(T(19+(-2+\kappa)\kappa)+8(-1+\kappa)\mu)X_2^2+3(T(-3+\kappa)+8\mu)(T+T\kappa+8\mu)X_2^4\right)+\\
&\quad 4X_1^2\left(18a^6T^2+2a^4T^2(14+\kappa(6+\kappa))X_2^2+a^2T(T(-21+(-2+\kappa)\kappa)+8(-1+\kappa)\mu)X_2^4+(T(-3+\kappa)+8\mu)(T+T\kappa+8\mu)X_2^6\right)\Big)
\end{aligned}
$$

## Body Load Components

### $F_1$

$$
\begin{aligned}
&-\frac{1}{64\mu^3(X_1^2+X_2^2)^8}a^2TX_1((64\mu^2((-1+\kappa)\lambda+(-3+\kappa)\mu)+\\
&\quad 16T\mu((5-3\kappa+\kappa^2)\lambda+(11-3\kappa+\kappa^2)\mu)+T^2((-3+9\kappa-3\kappa^2+\kappa^3)\lambda+(-21+17\kappa-\kappa^2+\kappa^3)\mu))X_1^{12}-\\
&\quad 2X_1^{10}(a^2T(8\mu((18-5\kappa+2\kappa^2)\lambda+(46-3\kappa+2\kappa^2)\mu)+T((2+25\kappa-5\kappa^2+2\kappa^3)\lambda+(-58+55\kappa+\kappa^2+2\kappa^3)\mu))+\\
&\quad (-64\mu^2((-1+\kappa)\lambda+(-3+\kappa)\mu)-16T\mu((-7-3\kappa+\kappa^2)\lambda+(-25-3\kappa+\kappa^2)\mu)+\\
&\quad T^2((27+15\kappa+3\kappa^2-\kappa^3)\lambda+(-3+55\kappa+\kappa^2-\kappa^3)\mu))X_2^2)+\\
&\quad X_1^8(2a^4T(24(8+\kappa)\mu(\lambda+3\mu)+T((48+53\kappa-\kappa^2+2\kappa^3)\lambda+(-112+139\kappa+13\kappa^2+2\kappa^3)\mu))-2a^2T\\
&\quad (8\mu(5(-6+7\kappa+2\kappa^2)\lambda+(-82+69\kappa+10\kappa^2)\mu)+T((466-7\kappa+35\kappa^2+10\kappa^3)\lambda+(934+23\kappa+89\kappa^2+10\kappa^3)\mu))X_2^2-\\
&\quad (320\mu^2((-1+\kappa)\lambda+(-3+\kappa)\mu)+16T\mu((97-15\kappa+5\kappa^2)\lambda+(271-15\kappa+5\kappa^2)\mu)+\\
&\quad T^2((129+189\kappa-15\kappa^2+5\kappa^3)\lambda+(-249+517\kappa-5\kappa^2+5\kappa^3)\mu))X_2^4)-\\
&\quad 4X_1^6(3a^6T(24\mu(\lambda+3\mu)+T((5+\kappa)^2\lambda+3(-3+10\kappa+\kappa^2)\mu))-\\
&\quad 2a^4T(24(6+\kappa)\mu(\lambda+3\mu)+T((250-11\kappa+5\kappa^2+2\kappa^3)\lambda+(414+19\kappa+15\kappa^2+2\kappa^3)\mu))X_2^2+\\
&\quad a^2T(8\mu((-78+55\kappa+10\kappa^2)\lambda+(-210+97\kappa+10\kappa^2)\mu)+\\
&\quad T((162-75\kappa+55\kappa^2+10\kappa^3)\lambda+(422-133\kappa+117\kappa^2+10\kappa^3)\mu))X_2^4+(320\mu^2((-1+\kappa)\lambda+(-3+\kappa)\mu)+\\
&\quad 16T\mu((37-15\kappa+5\kappa^2)\lambda+(91-15\kappa+5\kappa^2)\mu)+T^2((9+69\kappa-15\kappa^2+5\kappa^3)\lambda+(-129+157\kappa-5\kappa^2+5\kappa^3)\mu))X_2^6)+\\
&\quad X_1^4(36a^8T^2((11+2\kappa)\lambda+(5+6\kappa)\mu)+12a^6T(-72\mu(\lambda+3\mu)+T((-67-26\kappa+\kappa^2)\lambda+(-109-78\kappa+3\kappa^2)\mu))X_2^2+\\
&\quad 4a^4T(72(4+\kappa)\mu(\lambda+3\mu)+T((76+95\kappa+33\kappa^2+6\kappa^3)\lambda+3(-20+59\kappa+17\kappa^2+2\kappa^3)\mu))X_2^4-\\
&\quad 4a^2T(8\mu((-54+35\kappa+10\kappa^2)\lambda+(-154+69\kappa+10\kappa^2)\mu)+\\
&\quad T((-326-79\kappa+35\kappa^2+10\kappa^3)\lambda+(-610-193\kappa+89\kappa^2+10\kappa^3)\mu))X_2^6-\\
&\quad (1600\mu^2((-1+\kappa)\lambda+(-3+\kappa)\mu)+16T\mu((77-75\kappa+25\kappa^2)\lambda+(131-75\kappa+25\kappa^2)\mu)+\\
&\quad T^2((-171+129\kappa-75\kappa^2+25\kappa^3)\lambda+(-429+137\kappa-25\kappa^2+25\kappa^3)\mu))X_2^8)+X_2^2(648a^{10}T^2(\lambda+\mu)+\\
&\quad 36a^8T^2(-9\lambda+2\kappa\lambda+9\mu+6\kappa\mu)X_2^2+12a^6T(-24\mu(\lambda+3\mu)+T((-1-6\kappa+3\kappa^2)\lambda+3(-5-6\kappa+3\kappa^2)\mu))X_2^4+\\
&\quad 2a^4T(24\kappa\mu(\lambda+3\mu)+T((216-75\kappa+23\kappa^2+2\kappa^3)\lambda+(456-149\kappa+21\kappa^2+2\kappa^3)\mu))X_2^6-\\
&\quad 2a^2T(8\mu((42-25\kappa+2\kappa^2)\lambda+(102-31\kappa+2\kappa^2)\mu)+T((90+21\kappa-25\kappa^2+2\kappa^3)\lambda+(126-5\kappa-27\kappa^2+2\kappa^3)\mu))X_2^8-\\
&\quad 3(64\mu^2((-1+\kappa)\lambda+(-3+\kappa)\mu)+16T\mu((-3-3\kappa+\kappa^2)\lambda+(-13-3\kappa+\kappa^2)\mu)+\\
&\quad T^2((-19-7\kappa-3\kappa^2+\kappa^3)\lambda+(-5-31\kappa-\kappa^2+\kappa^3)\mu))X_2^{10})-2X_1^2(108a^{10}T^2(\lambda+\mu)-\\
&\quad 36a^8T^2((-7+2\kappa)\lambda+(-1+6\kappa)\mu)X_2^2-6a^6T(-72\mu(\lambda+3\mu)+T((-43-22\kappa+5\kappa^2)\lambda+(-133-66\kappa+15\kappa^2)\mu))X_2^4-\\
&\quad 4a^4T(24(2+\kappa)\mu(\lambda+3\mu)+T((-146+53\kappa+17\kappa^2+2\kappa^3)\lambda+(-358+67\kappa+19\kappa^2+2\kappa^3)\mu))X_2^6+a^2T\\
&\quad (8\mu((42-25\kappa+10\kappa^2)\lambda+(86-15\kappa+10\kappa^2)\mu)+T((-422-19\kappa-25\kappa^2+10\kappa^3)\lambda+(-946-157\kappa+5\kappa^2+10\kappa^3)\mu))\\
&\quad X_2^8+(448\mu^2((-1+\kappa)\lambda+(-3+\kappa)\mu)+16T\mu((-1-21\kappa+7\kappa^2)\lambda+(-31-21\kappa+7\kappa^2)\mu)+\\
&\quad T^2((-93-9\kappa-21\kappa^2+7\kappa^3)\lambda+(-75-97\kappa-7\kappa^2+7\kappa^3)\mu))X_2^{10}))
\end{aligned}
$$

## $F_2$

$$
\begin{aligned}
&-\frac{1}{64\,\mu^3\,(X_1^2+X_2^2)^8}\,a^2\,T\,X_2\,(3\,(64\,\mu^2\,((-1+\kappa)\,\lambda+(-3+\kappa)\,\mu)+\\
&\qquad 16\,T\,\mu\,((11-5\,\kappa+\kappa^2)\,\lambda+(29-9\,\kappa+\kappa^2)\,\mu)+T^2\,((-55+25\,\kappa-7\,\kappa^2+\kappa^3)\,\lambda+(-97+65\,\kappa-13\,\kappa^2+\kappa^3)\,\mu))\,X_1^{12}-2\,X_1^{10}\\
&\quad (a^2\,T\,(8\,\mu\,((60-27\,\kappa+2\,\kappa^2)\,\lambda+(156-37\,\kappa+2\,\kappa^2)\,\mu)+T\,((-340+137\,\kappa-31\,\kappa^2+2\,\kappa^3)\,\lambda+(-620+343\,\kappa-45\,\kappa^2+2\,\kappa^3)\,\mu))-\\
&\qquad (448\,\mu^2\,((-1+\kappa)\,\lambda+(-3+\kappa)\,\mu)+16\,T\,\mu\,((57-35\,\kappa+7\,\kappa^2)\,\lambda+(143-63\,\kappa+7\,\kappa^2)\,\mu)+\\
&\qquad\quad T^2\,((-265+135\,\kappa-49\,\kappa^2+7\,\kappa^3)\,\lambda+(-479+335\,\kappa-91\,\kappa^2+7\,\kappa^3)\,\mu))\,X_2^2)+\\
&\quad X_1^8\,(2\,a^4\,T\,(24\,(10+\kappa)\,\mu\,(\lambda+3\,\mu)-T\,((438-123\,\kappa+13\,\kappa^2+2\,\kappa^3)\,\lambda+(954-293\,\kappa-9\,\kappa^2+2\,\kappa^3)\,\mu))-\\
&\qquad 2\,a^2\,T\,(8\,\mu\,((108-35\,\kappa+10\,\kappa^2)\,\lambda+(284-45\,\kappa+10\,\kappa^2)\,\mu)+\\
&\qquad\quad T\,((-52+249\,\kappa-55\,\kappa^2+10\,\kappa^3)\,\lambda+(132+647\,\kappa-85\,\kappa^2+10\,\kappa^3)\,\mu))\,X_2^2+\\
&\qquad (1600\,\mu^2\,((-1+\kappa)\,\lambda+(-3+\kappa)\,\mu)+16\,T\,\mu\,((123-125\,\kappa+25\,\kappa^2)\,\lambda+(269-225\,\kappa+25\,\kappa^2)\,\mu)+\\
&\qquad\quad T^2\,((-463+321\,\kappa-175\,\kappa^2+25\,\kappa^3)\,\lambda+(-905+713\,\kappa-325\,\kappa^2+25\,\kappa^3)\,\mu))\,X_2^4)-\\
&\quad 4\,X_1^6\,(3\,a^6\,T\,(24\,\mu\,(\lambda+3\,\mu)+T\,((3-2\,\kappa+3\,\kappa^2)\,\lambda+(-91-6\,\kappa+9\,\kappa^2)\,\mu))+\\
&\qquad 2\,a^4\,T\,(-24\,(8+\kappa)\,\mu\,(\lambda+3\,\mu)+T\,((-72+9\,\kappa+7\,\kappa^2+2\,\kappa^3)\,\lambda+(-208-65\,\kappa-11\,\kappa^2+2\,\kappa^3)\,\mu))\,X_2^2+\\
&\qquad a^2\,T\,(8\,\mu\,((-12+25\,\kappa+10\,\kappa^2)\,\lambda+(-28+39\,\kappa+10\,\kappa^2)\,\mu)+T\,((356-27\,\kappa+5\,\kappa^2+10\,\kappa^3)\,\lambda+(828-37\,\kappa-\kappa^2+10\,\kappa^3)\,\mu))\\
&\qquad X_2^4-(320\,\mu^2\,((-1+\kappa)\,\lambda+(-3+\kappa)\,\mu)+16\,T\,\mu\,((3-25\,\kappa+5\,\kappa^2)\,\lambda+(-11-45\,\kappa+5\,\kappa^2)\,\mu)+\\
&\qquad\quad T^2\,((37+21\,\kappa-35\,\kappa^2+5\,\kappa^3)\,\lambda+(35+13\,\kappa-65\,\kappa^2+5\,\kappa^3)\,\mu))\,X_2^6)-\\
&\quad X_1^4\,(36\,a^8\,T^2\,(-27\,\lambda+2\,\kappa\,\lambda-9\,\mu+6\,\kappa\,\mu)+12\,a^6\,T\,(72\,\mu\,(\lambda+3\,\mu)+T\,((9-2\,\kappa+5\,\kappa^2)\,\lambda+3\,(-27-2\,\kappa+5\,\kappa^2)\,\mu))\,X_2^2+\\
&\qquad 4\,a^4\,T\,(-72\,(6+\kappa)\,\mu\,(\lambda+3\,\mu)+T\,((14-25\,\kappa+3\,\kappa^2+6\,\kappa^3)\,\lambda+3\,(-58-61\,\kappa-13\,\kappa^2+2\,\kappa^3)\,\mu))\,X_2^4+\\
&\qquad 4\,a^2\,T\,(8\,\mu\,(5\,(-12+9\,\kappa+2\,\kappa^2)\,\lambda+(-156+67\,\kappa+10\,\kappa^2)\,\mu)+\\
&\qquad\quad T\,((100-143\,\kappa+25\,\kappa^2+10\,\kappa^3)\,\lambda+(204-337\,\kappa+27\,\kappa^2+10\,\kappa^3)\,\mu))\,X_2^6+\\
&\qquad (-320\,\mu^2\,((-1+\kappa)\,\lambda+(-3+\kappa)\,\mu)-16\,T\,\mu\,((-57-25\,\kappa+5\,\kappa^2)\,\lambda+(-191-45\,\kappa+5\,\kappa^2)\,\mu)+\\
&\qquad\quad T^2\,((-397+99\,\kappa+35\,\kappa^2-5\,\kappa^3)\,\lambda+(-635+347\,\kappa+65\,\kappa^2-5\,\kappa^3)\,\mu))\,X_2^8)-X_2^2\,(-216\,a^{10}\,T^2\,(\lambda+\mu)+\\
&\qquad 36\,a^8\,T^2\,(\lambda+2\,\kappa\,\lambda+(-5+6\,\kappa)\,\mu)\,X_2^2-12\,a^6\,T\,(-24\,\mu\,(\lambda+3\,\mu)+T\,((13-2\,\kappa+\kappa^2)\,\lambda+(11-6\,\kappa+3\,\kappa^2)\,\mu))\,X_2^4+\\
&\qquad 2\,a^4\,T\,(-24\,(2+\kappa)\,\mu\,(\lambda+3\,\mu)+T\,((-2+21\,\kappa-11\,\kappa^2+2\,\kappa^3)\,\lambda+(-46+43\,\kappa-17\,\kappa^2+2\,\kappa^3)\,\mu))\,X_2^6+\\
&\qquad 2\,a^2\,T\,(8\,\mu\,((12-7\,\kappa+2\,\kappa^2)\,\lambda+(28-9\,\kappa+2\,\kappa^2)\,\mu)+T\,((-20+21\,\kappa-11\,\kappa^2+2\,\kappa^3)\,\lambda+(-28+43\,\kappa-17\,\kappa^2+2\,\kappa^3)\,\mu))\,X_2^8+\\
&\qquad (64\,\mu^2\,((-1+\kappa)\,\lambda+(-3+\kappa)\,\mu)+16\,T\,\mu\,((3-5\,\kappa+\kappa^2)\,\lambda+(5-9\,\kappa+\kappa^2)\,\mu)+\\
&\qquad\quad T^2\,((-7+9\,\kappa-7\,\kappa^2+\kappa^3)\,\lambda+(-17+17\,\kappa-13\,\kappa^2+\kappa^3)\,\mu))\,X_2^{10})-2\,X_1^2\\
&\quad (324\,a^{10}\,T^2\,(\lambda+\mu)+36\,a^8\,T^2\,((-5+2\,\kappa)\,\lambda+\mu+6\,\kappa\,\mu)\,X_2^2+6\,a^6\,T\,(72\,\mu\,(\lambda+3\,\mu)+T\,((-7+2\,\kappa+\kappa^2)\,\lambda+(-1+6\,\kappa+3\,\kappa^2)\,\mu))\\
&\qquad X_2^4+4\,a^4\,T\,(-24\,(4+\kappa)\,\mu\,(\lambda+3\,\mu)+T\,((188-47\,\kappa-5\,\kappa^2+2\,\kappa^3)\,\lambda+(348-89\,\kappa-15\,\kappa^2+2\,\kappa^3)\,\mu))\,X_2^6+a^2\,T\\
&\qquad (8\,\mu\,((-36+25\,\kappa+10\,\kappa^2)\,\lambda+(-100+39\,\kappa+10\,\kappa^2)\,\mu)+T\,((-244-99\,\kappa+5\,\kappa^2+10\,\kappa^3)\,\lambda+(-524-253\,\kappa-\kappa^2+10\,\kappa^3)\,\mu))\\
&\qquad X_2^8+(64\,\mu^2\,((-1+\kappa)\,\lambda+(-3+\kappa)\,\mu)+16\,T\,\mu\,((15-5\,\kappa+\kappa^2)\,\lambda+(41-9\,\kappa+\kappa^2)\,\mu)+\\
&\qquad\quad T^2\,((-79+33\,\kappa-7\,\kappa^2+\kappa^3)\,\lambda+(-137+89\,\kappa-13\,\kappa^2+\kappa^3)\,\mu))\,X_2^{10}))
\end{aligned}
$$

# DISTRIBUTION

| | | | |
|---|---|---|---|
| 1 | MS0346 | L.A.A. Heitman | 1553 |
| 1 | MS0346 | J.E. Bishop | 1556 |
| 1 | MS0557 | J. Pott | 1554 |
| 1 | MS0815 | J.S. Lash | 1500 |
| 1 | MS0840 | S.W. Attaway | 1500 |
| 1 | MS0845 | W.R. Witkowski | 1540 |
| 1 | MS0828 | A. Urbina | 1544 |
| 1 | MS0828 | B. Carnes | 1544 |
| 1 | MS0828 | K.J. Dowding | 1544 |
| 1 | MS0828 | S. Kieweg | 1544 |
| 1 | MS0828 | G.E. Orient | 1544 |
| 1 | MS0828 | J.R. Red-Horse | 1544 |
| 1 | MS0840 | J.M. Redmond | 1550 |
| 1 | MS0840 | H.E. Fang | 1554 |
| 1 | MS0840 | C.S. Lo | 1554 |
| 1 | MS0840 | K.D. Mish | 1555 |
| 1 | MS0840 | G.C. Duncan | 1555 |
| 1 | MS0845 | M.J. Skroch | 1542 |
| 1 | MS0845 | M.W. Heinstein | 1542 |
| 1 | MS0845 | J.D. Thomas | 1542 |
| 1 | MS0845 | K.H. Pierson | 1542 |
| 1 | MS0845 | D.M. Day | 1542 |
| 1 | MS0899 | Technical Library | 9536 (electronic copy) |

Sandia National Laboratories